Carderock Division, Naval Surface Warfare Center
Bethesda, Maryland 20084-5000

CDNSWC-SIG--94/021-7340 January 1994

Signatures Directorate
Research and Development Report

THREE-DIMENSIONAL SAR FROM CURVILINEAR APERTURES

by
Kenneth Knaell

CDNSWC-SIG-94/021-7340 Three-Dimensional SAR from Curvilinear Apertures

UNCLASSIFIED

SECURITY CLASSIFICATION OF THIS PAGE

REPORT DOCUMENTATION PAGE

Form Approved
OMB No. 0704-0188

1a. REPORT SECURITY CLASSIFICATION: UNCLASSIFIED	1b. RESTRICTIVE MARKINGS
2a. SECURITY CLASSIFICATION AUTHORITY	3. DISTRIBUTION/AVAILABILITY OF REPORT: Approved for Public Release; Distribution is Unlimited.
2b. DECLASSIFICATION/DOWNGRADING SCHEDULE	
4. PERFORMING ORGANIZATION REPORT NUMBER(S): CDNSWC-SIG-94/021-7340	5. MONITORING ORGANIZATION REPORT NUMBER(S)
6a. NAME OF PERFORMING ORGANIZATION: CDNSWC; 6b. OFFICE SYMBOL (If applicable): Code 7340	7a. NAME OF MONITORING ORGANIZATION
6c. ADDRESS (City, State, and ZIP Code): Bethesda, MD 20084-5000	7b. ADDRESS (City, State, and ZIP Code)
8a. NAME OF FUNDING/SPONSORING ORGANIZATION: Office of Naval Research; 8b. OFFICE SYMBOL (If applicable): 313	9. PROCUREMENT INSTRUMENT IDENTIFICATION NUMBER
8c. ADDRESS (City, State, and ZIP Code): 800 North Quincy Street, Arlington, VA 22217-5660	10. SOURCE OF FUNDING NUMBERS: PROGRAM ELEMENT NO: 601153N; PROJECT NO.: R1107; TASK NO: 206; WORK UNIT ACCESSION NO.: DN503432

11. TITLE (Include Security Classification)

Three Dimensional SAR From Curvilinear Apertures

12. PERSONAL AUTHOR(S)

Knaell, Kenneth K

13a. TYPE OF REPORT	13b. TIME COVERED	14. DATE OF REPORT (Year, Month, Day)	15. PAGE COUNT
Progress	FROM Oct93 TO Oct94	1994, Jan	39

16. SUPPLEMENTARY NOTATION

17. COSATI CODES			18. SUBJECT TERMS (Continue on reverse if necessary and identify by block number)
FIELD	GROUP	SUB-GROUP	imaging, clean, radar, deconvolution, SAR, superresolution

19. ABSTRACT (Continue on reverse if necessary and identify by block number)

Three-dimensional (3-D) radar imaging is presently at an exploratory stage of development. Such imagry is of proven usefulness and would undoubtedly find increased application if more readily available.

The 3-D information content in data taken from a curved SAR aperture is significant if sizable data projections are produced when the data are projected in three orthogonal directions. Such sparce data does not generate visually acceptable 3-D images by straight forward Fourier transformation however. The high sidelobes present in such images may be larger than major scatterers and thus veil their appearance and they also very nearly always interfere with visual lines of sight to other scatterers.

(See Reverse Side)

20. DISTRIBUTION/AVAILABILITY OF ABSTRACT: ☒ UNCLASSIFIED/UNLIMITED ☐ SAME AS RPT. ☐ DTIC USERS	21. ABSTRACT SECURITY CLASSIFICATION: UNCLASSIFIED
22a. NAME OF RESPONSIBLE INDIVIDUAL: Kenneth Knaell	22b. TELEPHONE (Include Area Code): (301)-227-1537; 22c. OFFICE SYMBOL: Code 7340

DISCLAIMER NOTICE

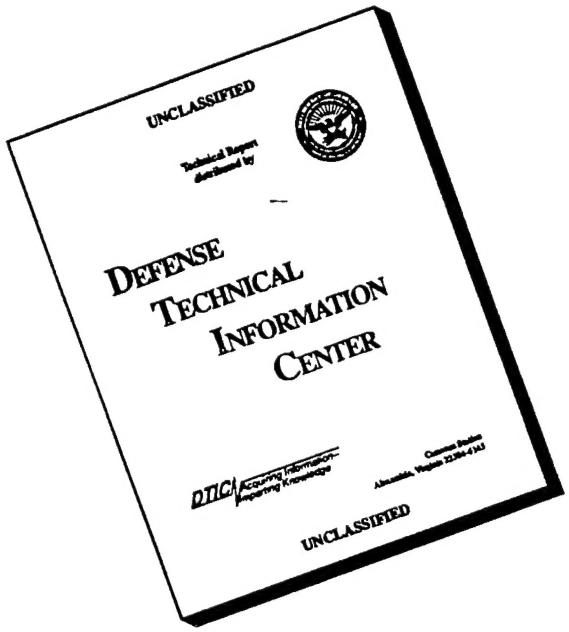

THIS DOCUMENT IS BEST QUALITY AVAILABLE. THE COPY FURNISHED TO DTIC CONTAINED A SIGNIFICANT NUMBER OF PAGES WHICH DO NOT REPRODUCE LEGIBLY.

(Block 19 Continued)
A coherent adaptation of the CLEAN algorithm is shown to be very effective in eliminating sidelobes in such images allowing the 3-D character of the target to be observed. Images obtained for a target consisting of eight corner reflector scatterers within several resolution distances of one another show only moderate dependence upon the aperture chosen. Comparison of results from real and simulated data indicate that the dynamic range available was not limited by sidelobe interferences in the subtractive deconvolution process but was inherent in the data in this experiment.

These results indicate that it may be possible to form visually useful 3-D images of targets in an operational situation from SAR data taken along a curvilinear aperture path.

CONTENTS

I - ABSTRACT

Three-dimenaional(3-D) radar imaging is presently at an exploratory stage of development. Such imagery is of proven usefulness and would undoubtedly find increased application if more readily available.

The 3-D information content in data taken from a curved SAR aperture is significant if sizable data projections are produced when the data are projected in three orthogonal directions. Such sparse data does not generate visually acceptable 3-D images by straight forward Fourier transformation however. The high sidelobes present in such images may be larger than the response for major scatterers and thus veil their appearance and they also very nearly always interfere with visual lines of sight to other scatterers.

A coherent adaptation of the CLEAN algorithm is shown to be very effective in eliminating sidelobes in such images allowing the 3-D character of the target to be observed. Images obtained for a target consisting of eight corner reflector scatterers within several resolution distances of one another show only moderate dependence upon the aperture chosen. Comparison of results from real and simulated data indicate that the dynamic range available was not limited by sidelobe interferences in the subtractive deconvolution process but was inherent in the data in this experiment.

These results indicate that it may be possible to form visually useful 3-D images of targets in an operational situation from SAR data taken along a curvilinear aperture path.

II - ADMINISTRATIVE INFORMATION

This investigation was performed at the Carderock Division of The Naval Surface Warfare Center (CDNSWC) in Bethesda, Maryland 20084-5000. The project was funded by Office of Naval Research (ONR 313). The work was funded through task number 206 of project number R1107 of program element number 601153N.

1 - INTRODUCTION

Three-dimensional (3-D) radar imaging is presently at an exploratory stage of development evidenced by a major thrust involving the recent joint effort of DARPA with the U.S. Army to develop a radar for geographic "Digital Terrain Elevation" models or contour maps by single pass interferometric synthetic aperture radar (IFSAR)[Appendix A]. Out of this activity, amounting to contracts of approximately $4,500,000 to industry, some effort was directed toward the development of target identification algorithms using the imagery from the radar specified in this acquisition.

Three-Dimensional images have been generated by processing data from surface radars located on Kwajelein Island in the South Pacific observing re-entry vehicles using inverse synthetic aperture radar (ISAR) methods. Images have also been made of the asteroid Castellia at a range of 5.7 million kilometers using data from the Cornell/Arecibo Radio Observatory in active radar mode [1.1]. Images of a similar type have also been obtained using raster-scanned antennas to synthesize a two-

dimensional synthetic aperture which; when combined with wide-band signals, can provide complete 3-D images.

Sub-optimal methods for approximating 3-D imaging include monochromatic holographic techniques and narrow-beam altimeter scanning. While the former offers excellent lateral resolution, it sacrifices the readily-acquired range information available from a frequency-diverse radar. Obtaining topographic details by scanning a narrow-beam altimeter over terrain features can also provide 3-D resolution but the lateral resolution is limited by the footprint of the antenna beam.

Methods requiring repetitive passes through a series of progressive look angles (raster scanned) produce a fully sampled or "filled" aperture. This combined with frequency diversity allows generation of 3-D images by standard Fourier transform techniques. Such methods however depend upon fortuitous geometric circumstances which are not practical in most operational scenarios. This obviously eliminates the application of such a method as illustrated in Figure 1.1 from battle or open field test situations.

The IFSAR system, while successfully producing images of smoothly varying terrain, suffers ambiguities when encountering steps in elevation. The effectiveness of such a system working at high resolution for target identification purposes or for the determination of positions of arbitrarily located scattering centers is uncertain. Further development along the lines of the above techniques may not lead to 3-D target identification methods useful in military applications.

The significant advantages offered by 3-D images of man made objects or of selected areas having military and commercial significance warrant the increased difficulty of their aquisition however. The benefits of images or even of clues to the 3-D characteristics of targets are well recognized in aerial photographic reconnaissance. The importance of this type of information for radar target detection and identification has been demonstrated as exemplified in [1.2]. Stereoscopic viewing methods have also been applied to synthetic aperture radar (SAR) ground image pairs to enhance interpretation[1.3].

The estimation of "hot spot" locations for radar cross-section diagnostic work on military vehicles made from 2-D images often requires educated guesswork in order to estimate the depth in the image at which the hot spot exists. Furthermore, as the radar cross-section of the target is reduced by supression treatment of these areas, the hot spots can become regions that are less easily identifiable as classical reflecting structures. Because the depth estimation process then becomes even more difficult, 3-D imaging would be of even further value for these applications.

This report describes a method which largely circumvents the severe shortcomings of the methods outlined above. The technique has been investigated and preliminary results are given. The results indicate that high resolution 3-D images may be obtained from data-sets generated by a radar carried on an aircraft flying a curved aperture path such as in Figures 1.2A and 1.2B. This technique is well suited to the imaging of objects consisting of finite numbers of isolated scattering centers typical of the target situations outlined above.

2 - BACKGROUND OF THE "COHERENT CLEAN" ALGORITHM

2.1 - GENERAL

As a result of emphasis upon the generation as opposed to visualization of 3-D images in this work, the viewpoint is taken that the array of numbers in storage in a computer constitutes the "image". The display of that array of numbers is of secondary importance to us here necessitated only by the need to evaluate how the imaging process is working. This visualization process is not part of the investiga-

tion that was undertaken. Fortunately a very useful 3-D visualization technique (SLICER) is available in the IDL programming environment and very little additional programming effort had to be expended to view results as they were obtained.

Throughout this paper a number of figures and mathematical derivations are presented in 2-D format for the sake of convenience. This should not be seen to detract from the validity of any conclusions that are made about 3-D results since the theoretical consequences of laborously adding the second cross range dimension to any of the derivations would add very little if any significance to the results obtained from the first cross range derivation. The 3-D results of most importance in this investigation result from the effectiveness of the CLEAN algorithm in forming images from the limited data presented to the algorithm.

2.2 - FOURIER IMAGE GENERATION

Corrections must be made to radar data in order to prepare it for image generation by means of Fourier transformation. That part of the process which determines its distribution into a matrix results from the character of radar data and the definition of the Fourier transform. It can be shown that the geometrical configuration of the area filled by actual measurements in the data or "transform" space bears a close relationship to the geometry of the measurement scenario in object space. If interpreted properly, angles in these two spaces transfer one to one although the units of linear measure are different.

As a result of this equivalency of angles it is very easy and informative to consider the regions where measured data are introduced into data space for various apertures that are traversed in object space. For this purpose a representation of the data space as in Figure 2.1 illustrating the spherical symmetry inherent in the data is useful. The radius of the sphere is proportional to the radar frequency and angles from the target to the radar are equal to the angles traced on the surface of the sphere. Thus a rolling ship observed by a stationary radar or alternatively a stationary ship observed by a radar on an aircraft doing rather aerobatic maneuvers might introduce data onto the sphere as shown.

Since a frequency diverse radar transmits a burst of many frequencies nearly instantaneously, theory dictates the line from the target to the radar at this moment define a parallel line in data space. The frequencies transmitted define distances along this line. Since the frequencies are repeated at all angles, concentric spherical shells are formed at these distances from the origin in data space. For clarity only one spherical shell and thus one frequency are represented in Figure 2.1. A small section of the spherical surface converted to rectangular coordinates with the frequencies reinstated is shown in the right drawing. For the ship a series of bursts and frequencies would produce a data surface perhaps similar to the sheet or ribbon shown in Figures 2.1 or 2.2A. For typical 2-D SAR operations the aperture is executed as closely as possible to a straight line and the sheet looks like Figure 2.2B. The 3-D images from these datasets are not useful in their basic form however. A horizontal cut through the 3-D image obtained from Figure 2.2B will produce the normal 2-D image obtained from this idealized linear aperture. The significance of this work however results from the fact that the proper treatment of the image from Figure 2.2A by the CLEAN algorithm will produce useful 3-D images such as are presented in section four of this document.

2.3 - CONVOLUTION IN THE RADAR IMAGE

A SAR image, regardless of its dimensionality, can be shown to be made up of the convolution of two other functions. The first function, the object (function) interrogated by the radar, is the radar reflectivity distribution of the object as a function of its coordinates. The second is a function characteristic of the measurement instrument along with the processing used to generate the image. The latter function, the point spread function (PSF), is independent of the object and is usually assumed

to be independent of its position in the image space (however for an object subtending a large angle as viewed from the radar this is not true).

An algebraic notation utilizing 'spatial frequency' is introduced which is useful when dealing with the radar round trip delay and the Fourier transform between range and frequency domains. The usual expression for the instantaneous phase along an electromagnetic wave where harmonic time variation is assumed is:

$$\phi = \underline{k} \bullet \underline{s} = \frac{2\pi}{\lambda} s \tag{1}$$

The dot product becomes the product of two scalars with the cosine of the included angle accounted for and the wavenumber is $k = 2\pi/\lambda$ (radian/meter).

The round trip phase from the radar to the target and back then produces a signal at the radar receiver represented by the phasor:

$$\exp\{j2\underline{k} \bullet \underline{s}\} = \exp\{j\frac{4\pi}{\lambda} s\} = \exp\{j2\pi f s\} \tag{2}$$

where 'spatial frequency' is defined: $f = 2/\lambda = 2f'/c$ (cycles/meter) and the usual temporal frequency is f'(cycles/second). Using this notation the range resolution is:

$$\rho = c/2\,BW' = c/2M\Delta f' = 1/M\Delta f \qquad \textit{where} \quad \Delta f = 2\,\Delta f'/c \tag{3}$$

Distance, s, can now be expressed as multiples, q, of ρ as:

$$s = q\ \rho = \frac{q}{M\,\Delta f} \qquad \textit{where} \quad \textit{q not necessarily an integer} \tag{4}$$

If the wave above is from a scatterer of complex amplitude, $g(\underline{s}_0)$, at position, $\underline{s}_0$, in Figure 2.3, then the radar datum from frequency step, k, of radar burst, i, is:

$$D_{ik} = g(\underline{s}_0)\ \exp\{-j2\pi\ \underline{f}_{ik} \bullet \underline{s}_0\} \tag{5}$$

where $\underline{f}_{ik}$ is the spatial frequency times the unit vector pointing to the radar along the LOS. The 2-D image is the inverse Fourier transform of this:

$$Im(\underline{s}) = \sum_i \sum_k D_{ik}\ \exp\{j2\pi\ \underline{f}_{ik} \bullet \underline{s}\} \tag{6}$$

or:

$$Im(\underline{s}) = g(\underline{s}_0) \sum_i \sum_k \exp\{j2\pi\ \underline{f}_{ik} \bullet (\underline{s} - \underline{s}_0)\} \tag{7}$$

Defining the PSF as:

$$PSF(\underline{s}) = \sum_i \sum_k \exp\{j2\pi\, f_{ik}\underline{s}\} \tag{8}$$

then:

$$Im(\underline{s}) = g(\underline{s}_0) \times PSF(\underline{s}-\underline{s}_0) \tag{9}$$

or:

$$Im(\underline{s}) = g(\underline{s}_0) \times \delta(\underline{s}-\underline{s}_0) \otimes PSF(\underline{s}) \tag{10}$$

where, $\otimes$, represents the mathematical convolution operation. Thus:

$$Im(\underline{s}) = g(\underline{s}) \otimes PSF(\underline{s}) \tag{11}$$

The result of this convolution process is generally to degrade the sharpness of the image; an effect analogous to the distorting procedure of passing a sharp electrical impulse through a narrowband electronic filter. The problem of reconstructing the original signal given the distorted waveform and the filter characteristic is equivalent to the imaging problem solved by the CLEAN algorithm. The imaging problem undertaken is that of obtaining the best estimate of the original object, which in this case is the CLEANed image, from the 3-D "DIRTY" image as shown in Figure 2.4. The DIRTY image is obtained by having measured the object with a narrow bandwidth radar and having processed this data with the straight forward Fourier transform, i.e. with a "diffraction limited", imaging process.

At this point it is important to emphasize that the microwave image which we are seeking to recreate from practically limited radar measurements may itself not look at all like an optical image of the target. Thus for critical evaluation of the effectiveness of the CLEAN process one should compare a CLEANed image with a microwave image, not an optical image. The most appropriate microwave image for comparison with a CLEANed image is one made from a "parent" dataset which includes, as a subset, the data used to form the CLEANed image itself. In this manner artifacts present in the CLEANed image that are also present in the image from the parent dataset (the ground truth for our purposes) can be identified as characteristic of the dataset and not due to the CLEAN process. Also since it is possible to form a CLEANed image from the full dataset as well as any subset, this is also a reasonable process with which to form a high quality image from the full dataset for evaluation purposes.

2.4 - CHARACTER OF THE PSF IN THE RADAR IMAGE

The application of the CLEAN algorithm to radar images has two characteristics distinguishing it from its application as originally proposed by Högbom for the enhancement of astronomical skymaps[2.1]. This was also recognized by Steinberg[2.2]. As a result of the complex valued nature of radar data and images, the phase at each step leading to the image must be properly processed. The second characteristic results from the fact that the radar image is generated from a narrow-band signal. This introduces a phase gradient into the PSF along the line of sight (LOS) to the radar whose aliased nature must be recognized.

Consider Equation (8) for the PSF. Defining the rectangular components of $\underline{s}$ as $\underline{s} = (x, y)$ and

those of f_{ik} as $f_{ik} = (f_0+k_x\Delta f\,,\, k_y\Delta f)$

where:

$$\begin{aligned} k_x &= -M/2\ ,\ \ldots\ ,\ M/2-1 \\ k_y &= -M/2\ ,\ \ldots\ ,\ M/2-1 \\ \Delta f &= \textit{spatial frequency sample spacing} \\ f_0 &= \textit{center frequency} \end{aligned} \tag{12}$$

then the dot product in (8) becomes:

$$\underline{s} \cdot f_{ik} = x(f_0 + k_x \Delta f) + y(k_y \Delta y) \tag{13}$$

Substituting into (8), the PSF becomes:

$$PSF = \frac{1}{M^2} \sum_{k_x=-M/2}^{M/2-1} \sum_{k_y=-M/2}^{M/2-1} \exp\{j2\pi [\, x(f_0 + k_x \Delta f) + y k_y \Delta f \,]\} \tag{14}$$

$$\begin{aligned} PSF = \exp\{j2\pi f_0 x\} \frac{1}{M} \sum_{k_x=-M/2}^{M/2-1} \exp\{j2\pi k_x \Delta f\, x\} \cdot \\ \frac{1}{M} \sum_{k_y=-M/2}^{M/2-1} \exp\{j2\pi k_y \Delta f\, y\} \end{aligned} \tag{15}$$

Now consider one of the above summations; letting:

$$r = \exp\{j2\pi \Delta f\, x\} \tag{16}$$

One of the sums in (15) can be written as:

$$S = \frac{1}{M} \sum_{k_x=-M/2}^{M/2-1} r^{k_x} \tag{17}$$

Let $k = k_x + M/2$ then:

$$S = \frac{1}{M} \sum_{k=0}^{M-1} r^{k-M/2} = r^{-M/2} \frac{1}{M} \sum_{k=0}^{M-1} r^k \tag{18}$$

But the geometric series:

$$\sum_{k=0}^{M-1} r^k = \frac{r^M - 1}{r - 1} \tag{19}$$

Then:

$$S = \exp\{j\pi M\Delta f\, x\}\ \frac{1}{M}\ [\frac{\exp\{j2\pi M\Delta f\, x\}-1}{\exp\{j2\pi\Delta f\, x\}-1}] \tag{20}$$

But:

$$\frac{e^{jM\theta}-1}{e^{j\theta}-1} = \frac{e^{jM\theta/2}\ (e^{jM\theta/2} - e^{-jM\theta/2})}{e^{j\theta/2}\ (e^{j\theta/2} - e^{-j\theta/2})} = e^{j(M-1)\theta/2}\frac{\sin(M\theta/2)}{\sin(\theta/2)} \tag{21}$$

Hence:

$$\frac{1}{M}\ [\frac{\exp\{j2\pi M\Delta f\, x\}-1}{\exp\{j2\pi\Delta f\, x\}-1}] = \exp\{j2\pi x(M-1)\Delta f\}\ \frac{\sin(M\pi\Delta f\, x)}{M\ \sin(\pi\Delta f\, x)} \tag{22}$$

and S becomes:

$$S = \exp\{-j\pi\Delta f\, x\}\ \frac{\sin(M\pi\Delta f\, x)}{M\ \sin(\pi\Delta f\, x)} \tag{23}$$

The sum over k_y produces a similar result. The PSF (15) can then be written:

$$PSF = [\frac{\sin(M\pi\Delta f\, x)}{M\ \sin(\pi\Delta f\, x)}.\frac{\sin(M\pi\Delta f\, y)}{M\ \sin(\pi\Delta f\, y)}]\ \exp\{j2\pi f_0 x\}\ \exp\{-j\pi\Delta f(x+y)\} \tag{24}$$

The term involving sine functions constitutes the envelope of the PSF with the two exponentials producing an internal phase gradient. If the bandwidths, MΔf, are equal in the range and (two) cross range directions as was assumed, the PSF has equal width in all three directions. The first exponential term is the phase gradient as a result of using a narrow band signal, i.e., a baseband signal offset by the frequency, f_0 . The last exponential term is the result of assumed assymetry in the data array (summation from -M/2 to M/2-1 instead of from -M/2 to M/2). This term is significant since x or y may be as large as (M-1)/MΔf. If M is odd and we put a sample at f_0 then this term disappears. In any case the error in phase by missing the peak in sampleing the image or the PSF is greater by a factor of $2f_0/\Delta f$ due to the preceeding exponential which is also a function of x.

2.5 - INTERPOLATION ERROR

In implementing the inverse Fourier transform by backprojection it is useful to obtain the value of range profiles on a finely sampled grid so that phase errors will be minimized. It is important to know the magnitude of this type of error as a function of grid size. Also phase errors due to pixel size exist in the final image. Since the cross range phase gradient is small or zero as shown above, the most significant error occurs as a result of the LOS phase gradient arrising from the carrier offset. Neglecting notation for burst number a radar datum may be written, combining Equations (4) and (5) as:

$$D_k(s) = g(s)\exp\{-j2\pi(f_s + k\,\Delta f)\frac{q}{M\Delta f}\} \tag{25}$$

where f_s is the lowest frequency transmitted, q is the noninteger dimensionless range of a point scatterer and:

$$k = 0, \ldots, M-1$$
$$M = \textit{number of frequencies transmitted} \tag{26}$$

For phase correct range profiles the shifted inverse Fourier transform is used:

$$P(r) = \exp\{j2\pi f_s r\}\sum_{k}^{M} D_k(s)\exp\{j2\pi k\,\Delta f\, r\} \tag{27}$$

For a discrete IFT the image coordinate is $r = n/M\Delta f$, thus:

$$P(\frac{n}{M\Delta f}) = g(\frac{q}{M\Delta f})\exp\{j\frac{2\pi f_s}{M\Delta f}(n-q)\}\sum_{k}^{M}\exp\{j\frac{2\pi k\Delta f}{M}(n-q)\} \tag{28}$$

or:

$$P(\frac{n}{M\Delta f}) = g(\frac{q}{M\Delta f})\cdot PSF(n-q) \tag{29}$$

Since the maximum value of (n-q) is 1/2, evaluating the first exponential in the above expression for the radar parameters used gives:

$$\textit{phase error} = \frac{2\pi f_0}{M\Delta f}\cdot\frac{1}{2}\cdot\frac{180}{\pi} = \frac{2\pi\cdot 10^{10}}{8192\cdot 47.625\cdot 10^6}\cdot\frac{1}{2}\cdot\frac{180}{\pi} = 4.5(\textit{degree}) \tag{30}$$

The phase error in sampling the range profile on a 8192 point grid is thus less than 4.5 degrees. The image however having only 32 samples to an edge would have a possible error 256 times this, i.e. one would have random errors in obtaining the phase from image samples used.

2.6 - THE CLEAN ALGORITHM

It was shown above that the radar image is the convolution of the PSF with a sharper function. The process to regain the sharper image is sometimes referred to as deconvolution. Since convolution in the image domain Fourier transforms to a product in the data domain, deconvolution in the image domain might be expected to be analogous to division in the data domain. Indeed undoing the effect of a tapered window applied to data across a frequency band can largely be undone by multiplying again by its reciprocal across the band. Thus in one consise operation every widened point response in the image would be made sharp again.

The data distribution shown in Figure 2.2A however has no thickness upon which to apply an unwindowing process. The data is either there or it is not and the sheet is only one sample thick. The blurred 3-D image from such a dataset can be generated however but it will be so cluttered with

sidelobes as to be useless in almost any situation. Even when a poor quality imaging system produces an image with a very high intensity peak however, it is a reasonable conclusion that the peak was the result of an isolated source at that location. One may even claim a point source if the peak has the characteristic shape of a point source response. Further, if the peak is of sufficiently high intensity, its location as well as amplitude and phase will be relatively unaffected by noise and other sources. We can conclude we know the location, amplitude, and phase of the point source responsible for that peak.

Knowing the position and complex amplitude of a point source and the PSF of the imaging system, it is possible to calculate the contribution made by the source to the entire image (mainlobe and sidelobes). This contribution (or a fraction of it) may be subtracted from the image, removing the peak (or reducing its size), leaving another peak as the highest peak[2.3, 2.4]. The process may then be repeated until all peaks above noise level are removed. One is finally left with uninteresting residue at the level of noise.

Each of the original image peaks will have generated a 3-D delta function at the location of its maximum point or a set of delta functions in that vicinity. Because of noise and interferences from other peaks, the maximum point of a peak may shift after partial removal. It is not possible to remove a peak exactly in one step because of these interferences. As a result of the above procedure the CLEAN algorithm is known as a subtractive deconvolution algorithm.

For visualization purposes a CLEAN image may be formed from these delta functions by convolving them with an artificial PSF of one's own choosing and having the desirable characteristics of narrow width and no sidelobes. It need only be wide enough to recombine in a single peak those delta functions associated with a point source. For other purposes the list of positions, amplitudes, and phases may be input to the process as needed.

The above algorithmic approach to deconvolution is predicated upon the assumption that each individual peak in a Fourier transform image resulted from a point source. If, as is usually the case, an individual peak is not due to a single point scatterer but to a collection of sources within a diffraction limited resolution cell, the CLEAN algorithm will make errors but it will assign multiple point sources to the peak and it will reduce the peak to a low residual level although we cannot remove the impact of the peak completely. At worst it will assign a collection of point scatterers to a peak, the precise scatterer locations having no significance but their convolution with an artifical PSF of sufficient width for visualization purposes producing a response similar to the diffraction limited image response. At best it will accurately isolate true point scatterers and isolated groupings of scatterers of size small in comparison to a diffraction limited spot. We expect the errors in positions, amplitudes, and phases as a result of sidelobe interference of neghboring scatterers to be minimal if the sources have disparate amplitudes and phases.

2.7 - COMPUTER PROGRAM

The program flow chart is shown in Figure 2.5. All programming was done in Research System's IDL programming environment running under XWINDOWS/UNIX on a DECSTATION 3100 with 24M Byte RAM. The diffraction limited images necessary for the CLEAN algorithm were generated by spherical backprojection. Spherical wave fronts were approximated by a four term Taylor's series. Initial experiments showed that 3-D images of 64x64x64 could be generated using the systems 3-D FFT package with memory swapping problems (thrashing) beginning to occur. This fact and the necessity to deal with the spherical wave front problem dictated using the spherical backprojection image generation process. For apertures containing small numbers (32 to 64) bursts of data, the global image formation process and the search for the global maximum took essentially equal amounts of time. The limit of a 32x32x32 image was set by run time for this particular computer. Planar wavefront data and a larger memory would allow a 3-D FFT to be used for image generation which would speed the

algorithm significantly. This would in turn allow 64x64x64 or larger images to be generated. A complex 32x32x32 image requires 256K bytes of storage while a 64x64x64 requires 2M bytes.

As a result of the small number of voxels possible in the 3-D image a maximization search procedure was implemented as opposed to subdividing the voxel size to reduce the phase error considered earlier. A search routine consisting of placing a 27 voxel sub-image at the global maximum and successively shrinking this while tracking the maximum was used. This had the added advantage of tracking hot spots to regions outside the initially specified image region to eliminate their sidelobe induced clutter within the space. Image formation in the 27 voxel subspace was also by spherical backprojection using discrete IFT's thus producing no interpolation error in the range profiles. This search could be made more efficient by using a six nearest neighbor search or a gradient search algorithm in future work.

CLEAN runs took from two hours to two days with typical runs taking two to six hours. By using FFT's and a more efficient search process this time could be reduced by perhaps an order of magnitude and a faster computer would decrease time accordingly.

The output of the CLEAN program is a list of positions, amplitudes, and phases of the various maxima revealed by the processing. The length of the list is equal to the number of CLEAN iterations. Also available is the original IFT (DIRTY) image and the image matrix left at the end of all iterations.

3 - EXPERIMENTAL METHOD AND RESULTS

Small corner reflectors were mounted on a framework of polystyrene foam about one half meter apart and were approximately two inches on an edge. The apertures used along with the number of bursts and the dynamic ranges achieved are shown in Figure 3.1. A planar approximation to spherical wavefronts and thus the possibility of image generation by inverse FFT was not attempted.

All of the results presented herein are for a target that consists of eight corner reflectors that form the corners of a cube. Tests on the other datasets obtained from Pacific Missile Test Center were discontinued as familiarity with the eight scatterer dataset became useful in interpretation of results. It was also the most crowded of the datasets available. The image resolution available from the bandwidth of the dataset as supplied was halved by truncation to produce a softer image. It could have been halved again and still have produced distinct scatterer identification as observation of the attendent images will attest. Such isolation would not be possible in 2-D images produced with similar resolution except for very selected orientations of the object relative to the image plane.)

The "dynamic range" was calculated by determining the amplitude value obtained in the progress of the CLEAN algorithm where peaks and thus point target responses were detected which did not lie in the vicinity of the known scatterer locations. These thus appeared as random scatterers and, whatever their cause, were considered the lower limit of useful image amplitude. The decibel ratio of this level to the peak amplitude in the original image is used as the dynamic range for purposes herein.

3.1 - SIDELOBE INTERFERENCE AND DYNAMIC RANGE

It appears that image degrading sidelobe interference (section 2.6) was not a factor in final CLEAN image quality for the particular configuration of eight scatterers and aperture configurations used. This significant finding is indicated by three observations regarding the dynamic range:

Simulated data was generated for a number of apertures. The positions of the eight point scatterers were derived from the coordinates of peaks determined from a CLEAN run on the full measured dataset. The result of comparison between CLEAN runs on real and simulated data is that the

dynamic range of runs on the simulated data consistantly progressed well beyond the 20db typical of the best runs on the real data. It is not likely that slight misplacements of the simulating scatterers would produce this result since several slight variations in the positioning produced the same results. Also errors in positioning were much less than the central lobe width of the PSF.

Secondly CLEAN runs on the full dataset and on various subapertures all had dynamic ranges from 15db to 20db fairly independent of the aperture configuration. If sidelobe interference were causing a serious problem it should have become less and the dynamic range correspondingly increased in the full dataset where the sidelobes were less extensive. This did not happen indicating sidelobe interference was not significant for this configuration of scatterers.

Thirdly the positions of the random peaks at the bottom of the dynamic range always appeared in the same general region of the image regardless of the subaperture configuration used. Interference from sidelobes and thus spurious scatterer locations would be expected to vary with the sidelobe structure resulting from different aperture configurations.

It was found that the 20db dynamic range was not extremely sensitive to aperture configuration and the number of bursts. Högbom[2.1] found that the number of baselines (bursts) affected final CLEAN image quality in skymap generation. A similar effect must occur in this application at some point. It appears that the lowest permissible number of bursts was not approached in our preliminary experimentation and that the simplicity of our image allowed therefore even the 32 burst minimum to serve well.

3.2 - AMPLITUDE VARIATION WITH IMAGE DECOMPOSITION.

In an image consisting of a single scatterer, the amplitude, a , of peaks successively removed by the CLEAN algorithm is:

$$a_{n+1} = a_n - g\,a_n \tag{31}$$

where g is the CLEAN "gain" factor and n the iteration number. The step change in a is then

$$\Delta a = a_{n+1} - a_n = -g\,a_n\,\Delta n \qquad \textit{where } \Delta n = 1 \tag{33}$$

Then:

$$\frac{\Delta a}{\Delta n} = -g\,a_n \tag{34}$$

The solution to this equation is:

$$a_n = a_0\,e^{-gn} \tag{35}$$

For small gains the CLEAN algorithm first attenuates one scattering center and as this is reduced to the value of the second peak it then alternates between these two. This process continues until it picks up a third and so on. As the removal of PSF's alternates between multiple peaks the combined attenuation rate is reduced by that multiplicity, M, thus for multiple scatterers Equation 35 becomes:

$$a_n = a_M e^{-gn/M} \tag{36}$$

In the absence of any noise and sidelobe interference one would thus expect a plot of the logarithm of amplitudes generated by the CLEAN algorithm to appear as in Figure 3.2.

Figure 3.3 shows the decrement in image amplitude peaks as a function of the CLEAN iteration number and Equation 36 plotted for several values of M for comparison. The initial slope exceeds or closely matches that for 8 scatterers and then gradually decreases to higher M values for more iterations. Since the eight scatterers were nearly matched in amplitude the smaller M values are not evident as would be expected. In addition this graph shows numerous positive increments as did similar plots for the smaller apertures. This behavior was not changed by lowering the gain factor. It is surmized that these persistant positive jumps and the increasingly high M character of the curve as a function of n are caused by the progressive removal of destructive sidelobe interference upon the eight major peaks. A more detailed understanding of this curve is in order. It is apparent from this and consideration of section 3.1 that the existing degree of sidelobe interference is not enough to produce serious imaging problems in a simple target. The variation of M as a function of n may be a useful indicator of image condition at any point in the CLEAN process.

Figure 3.4 is a histogram of amplitudes populating the 32x32x32 (32768) voxel image array before and after 25 iterations under the conditions of the previous CLEAN run. Filling in of many voxels by the low intensity residue of the 25 removed PSF's is apparent. The program run producing the data of Figure 3.4 was not carried to the 20db dynamic range level.

4 - ACCOMPLISHMENTS

A number of theoretical and computational issues were resolved allowing a computer program producing 3-D CLEAN images to be developed. Results from this program using very excellent data from Naval Air Warfare Center (formerly Pacific Missile Test Center) have produced very significant results related to the feasability of forming 3-D images by this technique. It was generally found that the CLEAN algorithm exceeded expectations, specifically in its immunity from significant sidelobe interference. It appears that the dynamic range of images generated from the excellent data were set by the clutter level in the data as opposed to limitations of the CLEAN imaging process. Sidelobe interference did not appear to seriously degrade final image quality although its effects were observed.

Also unexpected was the small number of bursts (32) that were more than sufficient to produce good images of this particular target scenario. The lower limit on this number was not determined but this result bodes well for the production of more complicated images.

The following images are made up of surfaces which are contours at constant amplitude (iso-contours) of a 32x32x32 image array. These surfaces are the 3-D equivalent to the closed contour lines of a 2-D contour map. The amplitude and therefore the size and complexity of these contours is set by input to the SLICER program. For thorough interrogation of an intricate image many renditions must be viewed varying this level and the view angle however the most revealing views were selected for presentation. Stereoscopic pairs were produced by incrementing the horizontal view angle six degrees between views. As a result of the unintended critical use to which the color prints are subjected by stereoscopic viewing, some depth misqueing is generated by the lack of proper registering of the surface textures between right eye and left eye views of the same scatterer.

Two techniques were used to generate a 32x32x32 array from the output list of the CLEAN algorithm. For quick results the amplitude, phase, and position of a single scattering center from the CLEAN list was added to the content of the single voxel encompasing that position. For more realistic (and perhaps statistically meaningful) results a 3-D Gaussian distribution of appropriate phase, amplitude and width was added into the total image centered on the coordinates from the list.

Figure 4.1 shows the orientation of the coordinate axes in the SLICER representations.

Figure 4.2 represents the IFT of the full 32x32x32 dataset. Sidelobes are evident in the three cardinal directions from the brightest scatterers. Figure 4.3 represents application of a raised cosine window to the above dataset. Tese images may be regarded as the ground truth which the CLEAN algorithm seeks to recover from any subset of this data.

Figure 4.4 represents the IFT (DIRTY) image resulting from the sinusoidal aperture of Figure 3.1A. The eight scatterers are unquestionably lost in the sidelobe clutter of this image. Figure 4.5 is a view, showing the downrange coordinate (LOS) from right to left, of the IFT (DIRTY) image resulting from the circular aperture of Figure 3.1C. This crossrange view illustrates the full downrange resolution of the frequency diverse radar typical of the curvilinear datasets. Although the crossrange distribution of sidelobes show circular symmetry they are scattered over the full image frame and beyond. Figure 4.6 represents the result of application of the CLEAN algorithm to Figure 4.4. The eight scatterers are clearly in evidence in reasonably correct orientation. Some amplitude distortion is evident which appears to be aperture dependent. This image was generated using the single pixel fill technique. Movement of CLEAN generated peaks among adjacent pixels for each of the eight scatterers combined with smoothing inherent in the SLICER program results in the nearly spherical scatterer responses.

Figure 4.7 is a stereographic representation of the IFT of the full 32x32x32 dataset. It is equivalent to Figure 4.2 with a lower contour level. Figure 4.8 is a stereographic representation of the CLEANed image of Figure 4.5 (circular aperture). This image was generated using the Gaussian fill technique.

Application for patent protection on the principles utilized in this imaging technique has been initiated.

5 - QUESTIONS REMAINING

The question of practicality demands knowing the level of adversity at which this technique will continue to work. If this limit can be extended by using more data then this question may be equivalent to the following one.

What is the requirement (similar to that investigated by Högbom) for sufficient number of bursts as a function of image complexty in differing situations (differing apertures, noise levels, etc.)? In a high clutter situation how many bursts or what other requirements must be satisfied to obtain satisfactory images. Is there an optimum aperture in this limit?

In order to obtain highly focused images the positions of the platform upon which the radar antenna is mounted must be known within a fraction of a wavelength. Are inertial nagivation systems (INSs), perhaps combined with global positioning system information, capable of giving sufficiently accurate position information of the aperture path in the highly curved aperture (high-G) environment? If the upper peaks of the serpentine aperture as illustrated in Figure 1.2A are made parabolic, it is possible to have the INS in free fall conditions over these parts of the path. This may allow an improvement in INS accuracy if required.

6 - NEXT STEPS

It is believed that the computer program developed is a good framework upon which to proceed to other (speeded up) versions.

The final usefulness of this technique will undoubtedly in part be determined by its robustness in real situations and therefore a necessary path to take is to advance to more realistic targets in more realistic scenarios. At this point it would be wise to avoid questionable data which, when combined with a complicated target, might give disappointing and difficult to interpret results. The integrity of the look angle measurements is as important as the radar output itself. With good data any target could be imaged as a next step however interpretation would be facilitated by using only a modestly complex target. One or a limited number of known multiple bounce reflections and a few moving glint points would be desirable in this next step which might be satisfied by a target drone in certain orientations. Planar wavefront data would be helpful.

The effect of close-in (ground or sea) clutter should be investigated, preferably in a series of imaging steps progressing from a corner reflector array to a vehicle or model in these surroundings. The loss of coherence in a tree canopy penetration image would finally be appropriate. Data quality should not be sacrificed in these more complicated experiments so it would be desirable to do these in a turntable or similarly controlled situation.

The CLEAN response to non-point scatterers alluded to at the beginning of Section 2.6 was not severly tested with the dataset used since groupings of maxima were always localized to the regions where the eight primary scatterers were known to exist. It would be useful to determine the response to interfering scatterers at resolution cell size spacing and to moving glint points under controlled conditions. Understanding of these effects on CLEAN operation would prove helpful in real imaging.

At this point it would be useful to determine the precise capabilities of inertial guidance systems (INSs) in this application. Contrary to what might be expected this information may not be easily obtainable from possible suppliers. This is an unusual application for even SAR optimized INS systems and users have historically had to adapt commercially available navigational units to suit their measurement needs.

Computational limitations were approached in the present investigation. The scope of work could be accelerated at this point by incorporation of extra manpower or industrial support to handle a broader scope of data acquisition and processing activity.

7 - CONCLUSION

The CLEAN algorithm operaated extremely well in this preliminary investigation. Three dimensionsal (I)SAR images have now been generated from practically executable apertures. The next step is to find the limitations of this technique.

8 - ACKNOWLEDGMENT

The author would like to thank Dean Mensa for the many informative and encouraging discussions and for providing the data that made this work possible. He would also like to thank Glen Heidbreder for the mathamatical results and much discussion relative to them which provided the insight into the nature of a radar image necessary to make a coherent implementation of CLEAN work.

9 - REFERENCES

[1.1] Eberhart, J., "Radar Reveals an Asteroid's Strange Shape", Science News, Nov.25,1989, p343.

[1.2] Steinberg, Bernard D. and Kang, Bonsoon, "Radar Detection Sensitivity as a Function Of Target Dimensionality", IEEE International Radar Conference, 1990, Proceedings, p106.

[1.3] Fullerton, Kevin J., Leberl, Franz, and Marque, Robert E., "Opposite-Side SAR Image Processing for Stereo Viewing", Photogrammetric Engineering and Remote Sensing", Vol 52, No.9, September 1986, pp1487-1498.

[2.1] Högbom, J.A.,"Aperture Synthesis with a Non-Regular Distribution of Interferometer Baselines", Astron. Astrophys. Suppl., Vol. 15(1974), pp417-426.

[2.2] Tsao, Jenho, and Steinberg, Bernard D.,"Reduction of Sidelobe Artifacts in Microwave Imaging", IEEE Tran.Ant.and Prop'n, Vol36, No4, April 1988, pp543-556.

[2.3] Clark, B.G.,"An Efficient Implementation of the Algorithm 'CLEAN'", Astron. Astrophys. Vol. 89(1980), pp377-378.

[2.4] Styerwalt, D. and Heidbreder, G., "On a Bayesian Approach to Coherent Radar Imaging", Maximum Entropy and Bayesian Methods, Kluwer, Dordrecht, 1992

10 - APPENDIX A

WEDNESDAY
March 4, 1992

COMMERCE

Issue No. PSA-054

A daily list of U.S. Government procurement invitations, contract awards, subcontracting leads, sales of surplus property and foreign business opportunities

BUSINESS DAILY

U.S. GOVERNMENT PROCUREMENTS

The Commerce Business Daily publishes, for Federal agencies, synopses of proposed contract actions that exceed $25,000 in value.

Services

A Research and Development

Directorate of R&D Contracting WPAFB OH 45433-6503

A -- THREE-DIMENSIONAL INTERFEROMETRIC SYNTHETIC APERTURE RADAR (IFSAR) SOL PRDA NO. 92-05-AAK DUE 042092 POC Contact Philip Porter, Contract Negotiator, (513) 255-2902. Wright Laboratory (WL/AAR) is interested in receiving proposals (technical and cost) on the research effort described below. Proposals in response to the PRDA shall be submitted by 20 Apr 92, 15:00 hours addressed to Wright Laboratory, Building 7, Area B, ATTN: (Mr Philip Porter, WL/AAKR) Wright Patterson AFB OH 45433-6503. Proposals submitted shall be in accordance with this announcement. LATE PROPOSALS: Proposal submission after the cut off date specified herein shall be treated IAW restriction at FAR 52.215-10, a copy of this provision may be obtained from the procuring office. This PRDA may be amended to allow subsequent submission of proposal dates. There will be no Format Request for Proposal or other solicitation request in regard to this requirement. Offerors should be alert for any required PRDA amendments that may be published. Offerors should consider instructions contained in the "Proprietary Information" and "When and How to Submit Proposals" sections of the Air Force Systems Command Unsolicited Proposal Guide, AFSC Pamphlet 70-5, copies of which are available by writing to HQ AFSC/DAPL ANDREWS AFB, D.C. 20334-5000, 301 981 2596 ADDRESS FOR AFSC PAMPHLET 70-5. AFSC Form 91, Policy Agreements, do not apply to PRDAs. Proposal preparation should follow all guidance found in the above-referenced sections of AFSC Pamphlet 70-5, except for guidance which could only be applied to unsolicited proposals, e.g., paragraph 6.d. The accompanying cost proposal/price breakdown shall be supplied on an SF 1411, together with supporting schedules, and shall contain a person hour breakdown per task. Copies of the above-referenced forms may be obtained from the contracting office cited. Proposals must be submitted in an original plus five copies. The selection of one or more sources for contract award will be based on a scientific and/or engineering evaluation of offerors' responses (both technical and cost aspects) to determine the technical merit of your proposal in response to the announcement. Technical merit, which is ranked as the first order of priority, shall be evaluated based upon the following criteria which are of equal importance. (a) new and creative solutions, (b) the offeror's understanding of the scope of the technical effort, (c) soundness of offeror's technical approach, (d) the availability of qualified technical personnel and their experience with applicable technologies, (e) the offeror's past experience with applicable synthetic aperture radar (SAR), three dimensional (3-D) SAR and interferometry radar technologies. Cost is ranked as the second order of priority. No other evaluation criteria will be used. The technical and cost information will be evaluated at the same time. The technical proposal shall be limited to 100 pages (12 pitch or larger type, double spaced, single sided, 8.5 by 11 inches), and must include a discussion of the nature and scope of the research and the technical approach. Additional information on prior work in this area, descriptions of available equipment, data and facilities, and resumes of personnel who will be participating in this effort should also be included as attachments to the technical proposal and are not included in the page limit. The goal for cost proposals is not more than 75 double spaced, double sided pages. The technical proposal and cost proposal shall be in separate volumes. Proposals should reference the above PRDA number. The Air Force reserves the right to select for award any, all, part or none of the proposals received. The contractor's proposal shall include a Statement of Work detailing the technical task proposed to be accomplished under the proposed effort and suitable for contract incorporation. The Statement of Work shall be prepared in accordance with MIL-HDBK 245B. Any questions concerning Statement of Work preparation shall be referred to the AF Project Engineer cited in this announcement. This announcement is an expression of interest only and does not commit the Government to pay for any response preparation cost. The cost of preparing proposals in response to this PRDA is not considered an allowable direct charge to any resulting or any other contract. It is, however, an allowable expense to the normal bid and proposal indirect cost as specified in FAR 31.205-18. Specific technical requirements and other information follows: B-(1) REQUIREMENTS: New and innovative approaches are sought to assess the value of the use of 3-D SAR signatures for detection and recognition of fixed and mobile, militarily significant objects. It is anticipated that the approach would include algorithm development and evaluation, parametric tradeoffs, data collection, and field demonstration. The exploration of interferometric SAR techniques may be evaluated in conjunction with other detection/recognition techniques including polarimetric SAR. Applications for 3-D IFSAR include forward-looking for weapon delivery, side-looking radar for small-area reconnaissance and/or long range standoff wide area search and cue. Due to the compressed time period of the effort, based on available funding, it would be expected that existing equipment would be used with minor modifications. (2) Deliverable Items: The following deliverable data items shall be required: (a) R&D Status Report, DI-A-3002A/T, monthly, (b) Funds and Manhour Expenditure Report, DI-FNCL-80331/T, monthly, (c) Project Planning Chart, DI-MGMT-80507A/T, monthly, (d) Contract Funds Status Report (CFSR), DD-1006B/T, quarterly, (e) Presentation Material, DI-3024A/T, as required, (f) Informal Technical Information Contractor's Bating Voucher, DI-S-30593/T, monthly, (g) Scientific and Technical Reports, DI-MISC-80711/T, (Draft and Reproducible Final), (3) Total contract Period Anticipated: The total length of the technical effort is estimated to be 24 months. The contractor shall also provide for an additional 4 months for processing/completion of the final report. (4) Expected Award Date: 1992 April - June. (5) Government Estimate: The government anticipates a target of $4,500,000 per contract award is anticipated. (6) Type of Contract: Cost Plus Fixed Fee (CPFF). (7) Security Requirement: It is anticipated that work performed under this contract may be classified up to and including the SECRET level. A cleared tempest approved processing facility is required for all proposals where classified information is to be processed. (8) Government Furnished Equipment: It is the offeror's responsibility to identify and arrange for use of any equipment be it contractor-owned and furnished or government-owned and furnished. (9) Size Status: Firms responding should indicate whether they are or are not a socially and economically disadvantaged business, whether or not they are woman-owned business, and should also indicate their size status. For the purpose of this acquisition, the size standard is 500 employees (SIC 8731). (10) Notice to Foreign Owned Firms: Foreign and foreign-owned firms are restricted for participation as a prime contractor. Any subcontracting arrangements shall be handled in accordance with the International Traffic in Arms Regulation (ITAR). (11) ITARS: International Traffic in Arms Restrictions apply. (12) A Briefing to Industry will be held at the Topographic Engineering Center, U.S. Army Corps of Engineers, Ft Belvoir VA, approximately two weeks from the publication date of this announcement. For further information contact Richard Koesel, Wright-Patterson Air Force Base, OH 45433-6543, 513-255-6427. The Briefing to Industry will be limited to personnel holding an active SECRET clearance. Attendees are required to forward their intention to attend the briefing and their security clearance information no later than 10 days from the publication of this announcement to USATEC, ATTN: CETEC-SO, CODE 2592, Ft Belvoir VA 22060-5546, FAX: 703-355-3176. This briefing will also include a discussion of U.S. Army interests in IFSAR for digital terrain elevation measurement, synopsized in a separate CBD announcement from the Topographic Engineering Center, U.S. Army Corps of Engineers. (13) PRDA Contact Point: Questions on technical issues may be referred to the Project Engineer, Richard Koesel, Wright-Patterson Air Force Base, OH 45433-6543, 513-255-6427. Questions related to contract/cost issues should be directed to Directorate of Research and Development Contracting, Philip Porter, Wright-Patterson Air Force Base, OH 45433-6503, 513-255-5[illegible]. Offerors are advised that only contracting officers are legally authorized to commit Government. All responsible sources may submit a proposal which shall be considered by the agency. (0062)

WL/PK, Wright-Patterson AFB, Ohio 45433-6503

A -- LIGHT WEIGHT DIMENSIONALLY STABLE MATERIALS SOL F33615-92-R-5905 DUE 031992 POC Phil Nelson, Contract Negotiator, (513) 255-5051; Frederick Rueth, Contracting Officer, (513) 255-5051; Lt. Jeff Guthrie, Project Engineer, (513) 255-9058. This directorate intends to issue Request for Proposal F33615-92-R-5905 on or about 92 Mar 19. Requests for a copy of the solicitation should be received, in writing, later than 15 days from the date of this listing in the Commerce Business Daily. Telephone requests will not be honored.--The objective of this program is to develop and demonstrate dimensionally stable, light weight materials, attachments, joining and assembly technologies for large space subsystems (fixed and deployable), such as phased array antenna backup structures, spacecraft bus structures, optical benches, solar power backup structures, and advanced thermal management systems. The program will establish preliminary materials and process specifications for joining and assembly of C-C composite materials, generate engineering and design type data on representative joint assemblies and evaluate analytic methods for modeling joint behavior for maximum performance at minimum weight. These efforts will provide the necessary experience and data base for joining and assembly of C-C required to facilitate their use in future space systems. Teaming arrangements are encouraged and, if the prime contractor/offeror is not a prime for a space platform with potential C-C applications, he shall work with a "space platform" contractor for such a system throughout the program to maintain relevancy of the proposed concepts and to meet realistic requirements. The program will consist

Content

SUBSCRIPTION INFORMATION

$261 a year (First Class mailing), $208 a year (Second Class mailing).
6 Month Trial Subscription: $130 (First Class), $104 (Second Class).
Foreign Rate: $250 a year - $130 six months, plus Air Mail rates.
Two year subscription available at above yearly rates.

To Order, Send remittance with full mailing address to the Superintendent of Documents, Government Printing Office, Washington, DC 20402-9371, Tel. 202/783-3238 fax 202/512-2233. Purchase order must be accompanied by payment. Make check payable to Superintendent of Documents. Visa or Master Card are acceptable. Allow approximately 6 weeks for delivery of first issue.

Service problems, Call Superintendent of Documents, Government Printing Office Washington, DC, Tel. 202/512-2303 or fax 202/512-2168.

Expiration, Subscriptions expire one year from the date of the first issue. One expiration notice is mailed about 90 days before expiration date.

Address Changes, Send to Superintendent of Documents, Government Printing Office Washington, DC 20402-9373, with entire mailing label from last issue received.

Reader's Guide

The Reader's Guide is published, on the last three pages, in every Monday edition of the Commerce Business Daily (CBD). The Reader's Guide includes the CBD's Numbered Notes, an Index of the Classification Codes and other information. If the Monday edition of the CBD is not printed because of a holiday, the Reader's Guide will appear in the next day's issue.

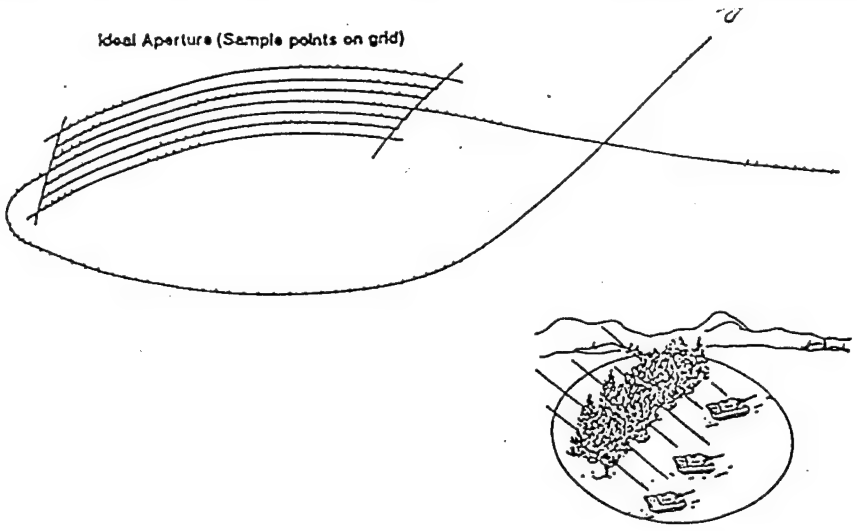

Fig. 1.1 Ideal aperture for 3-D, impractical

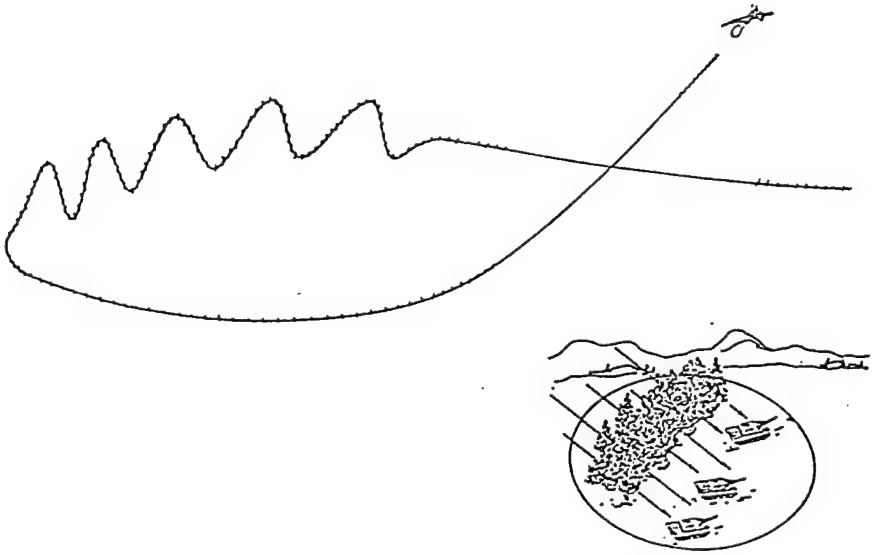

Fig. 1.2A Practical 3-D aperture, possible stripmap mode.

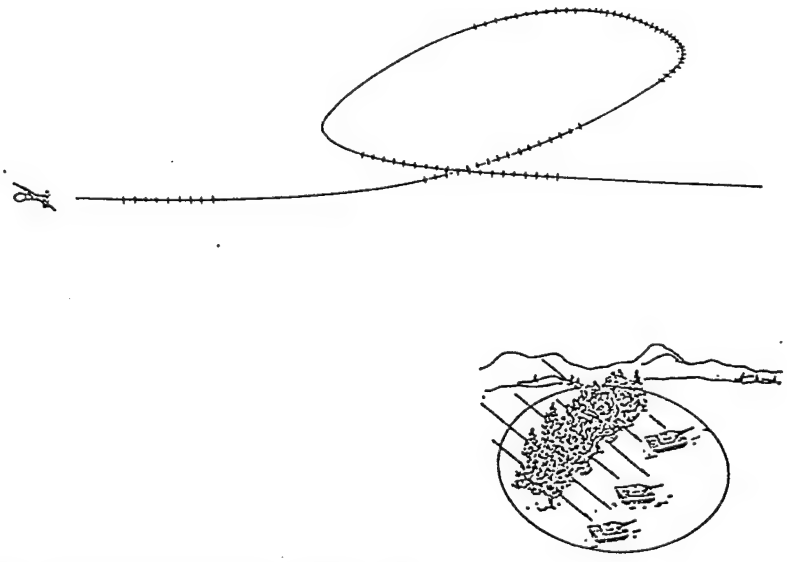

Fig. 1.2B Practical 3-D aperture

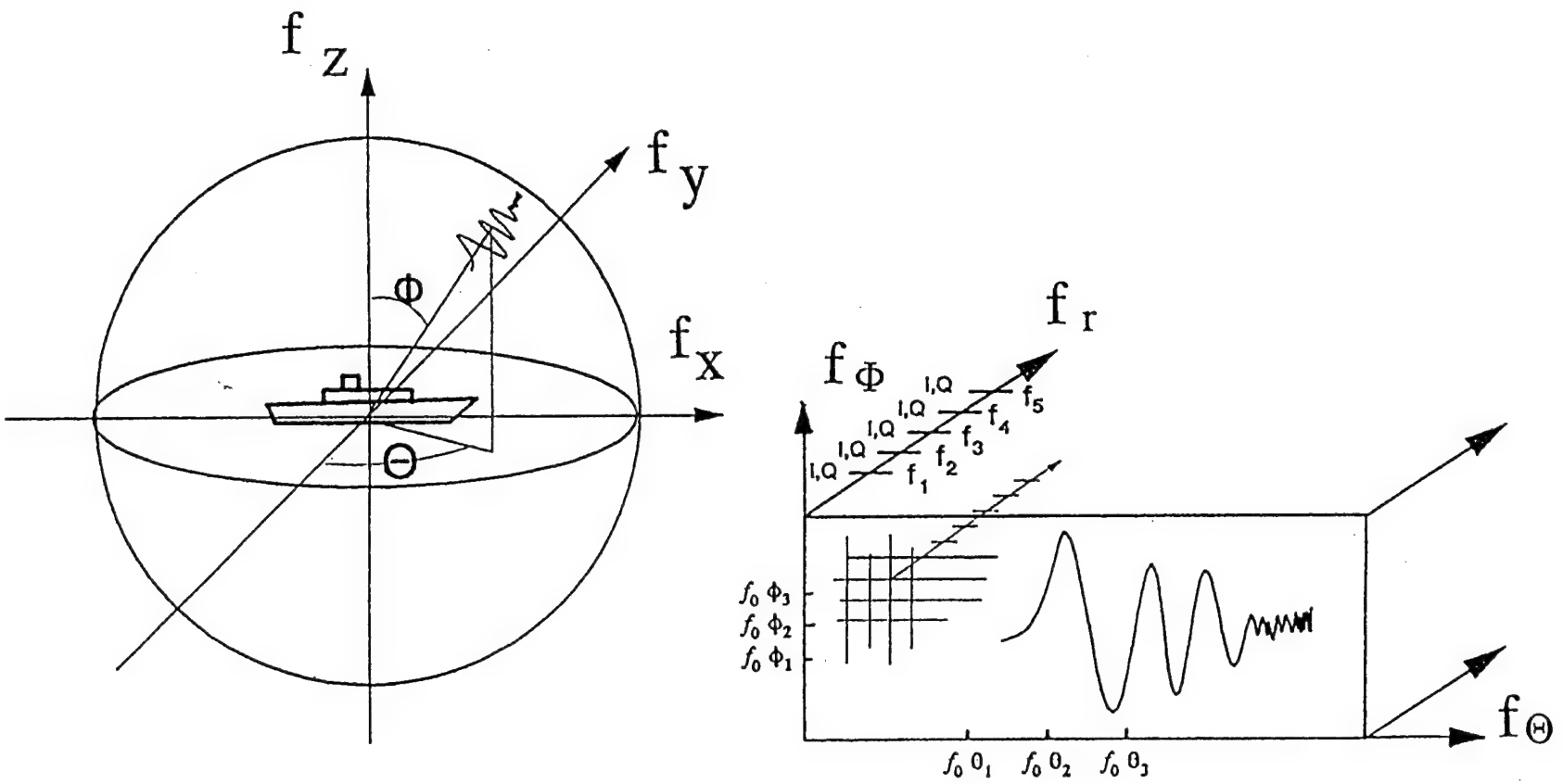

Fig. 2.1 Radar data in frequency space

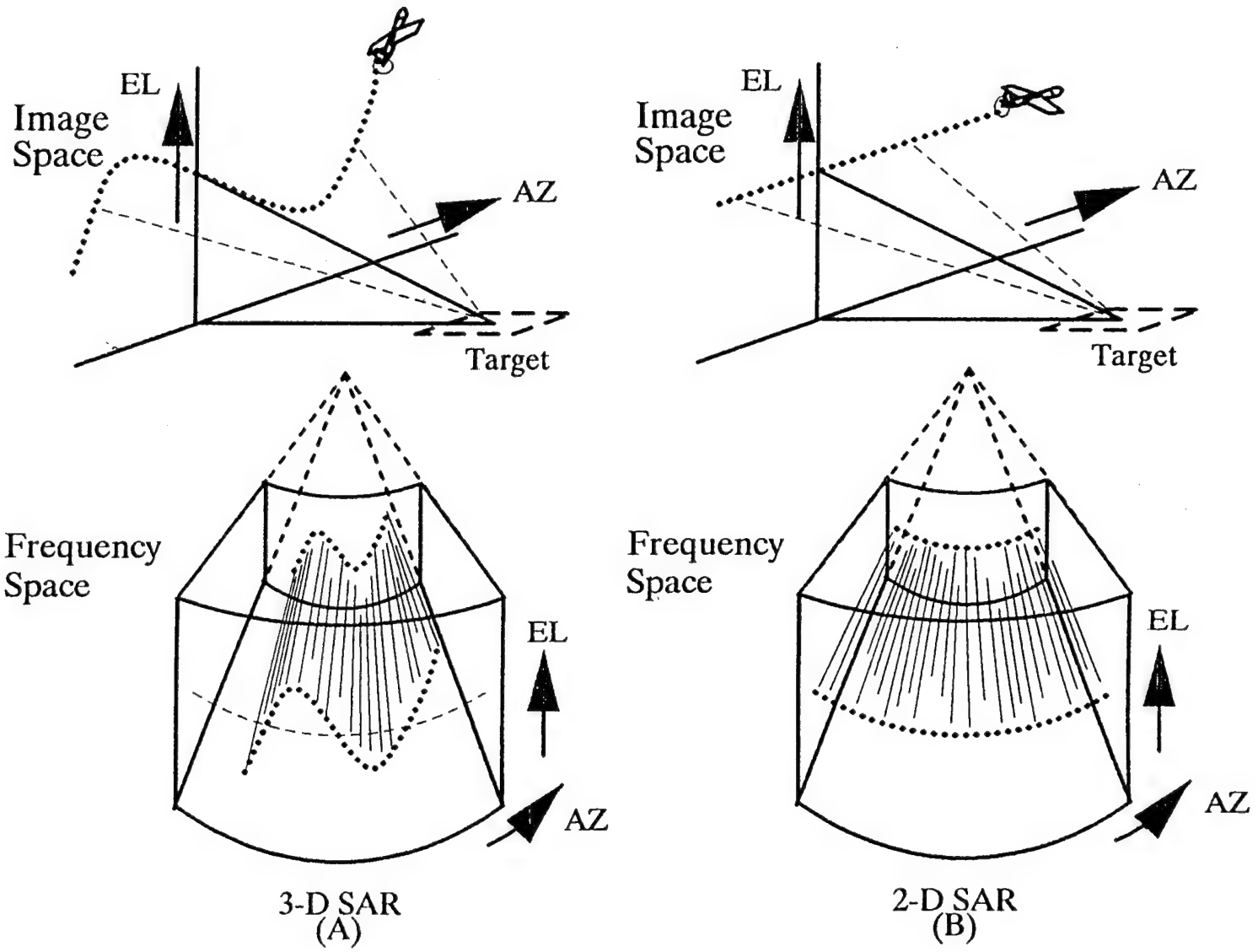

Fig. 2.2 Relationship between aperture path and data space support

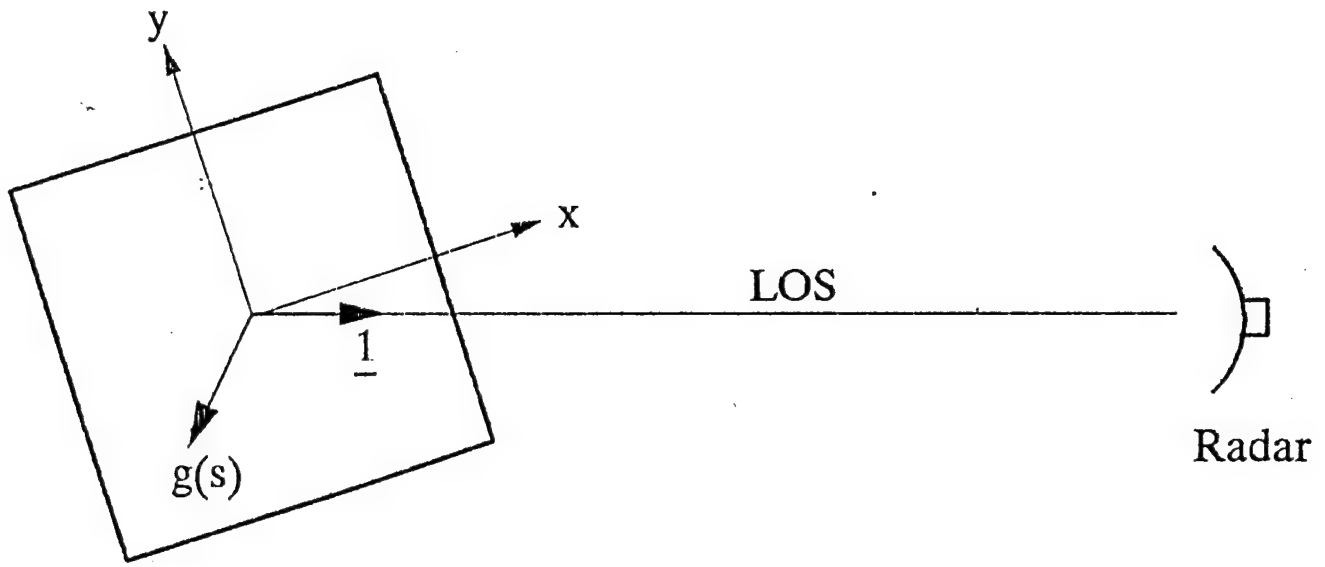

Fig. 2.3 Radar in target based coordinate system.

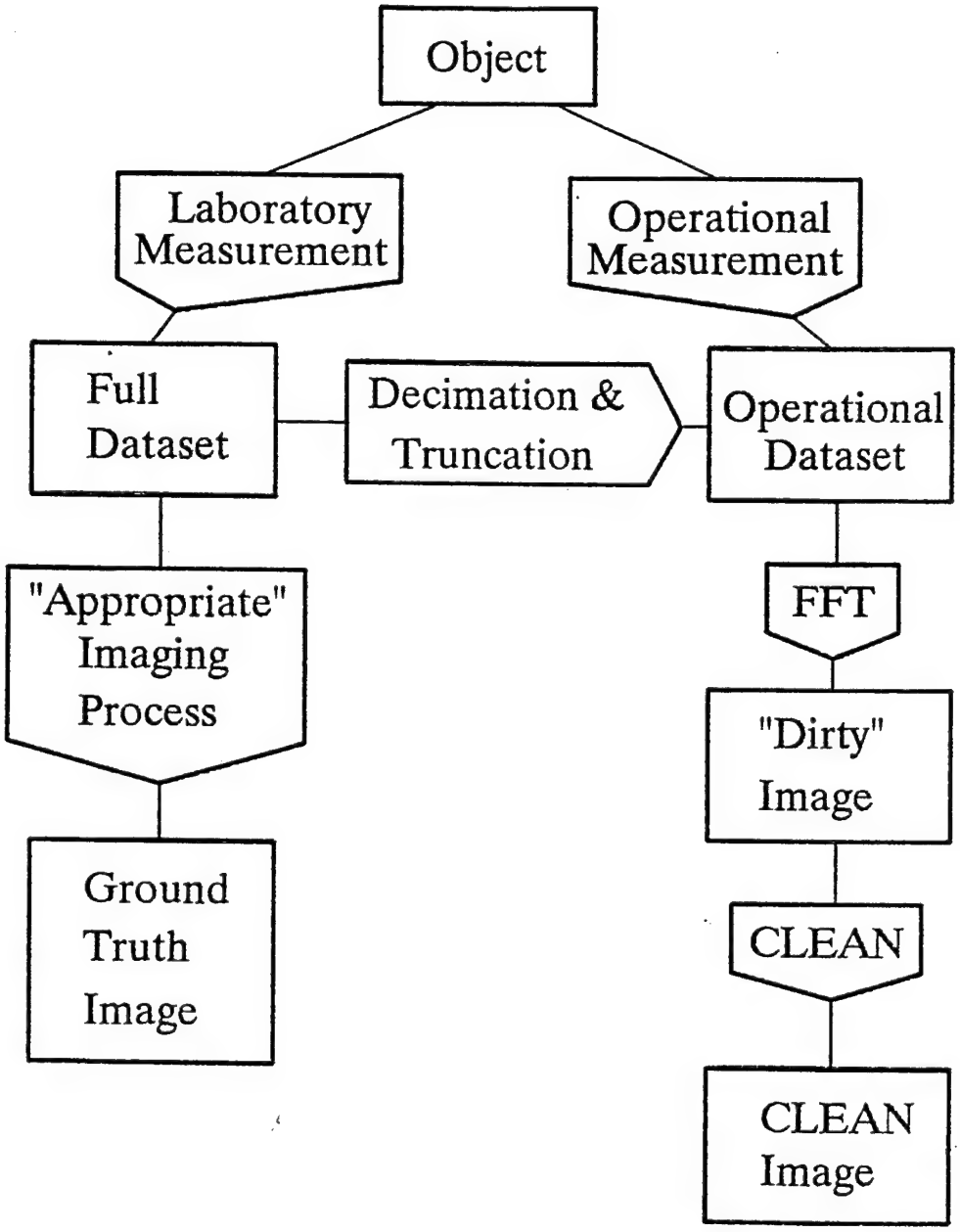

Fig. 2.4 Data Flow

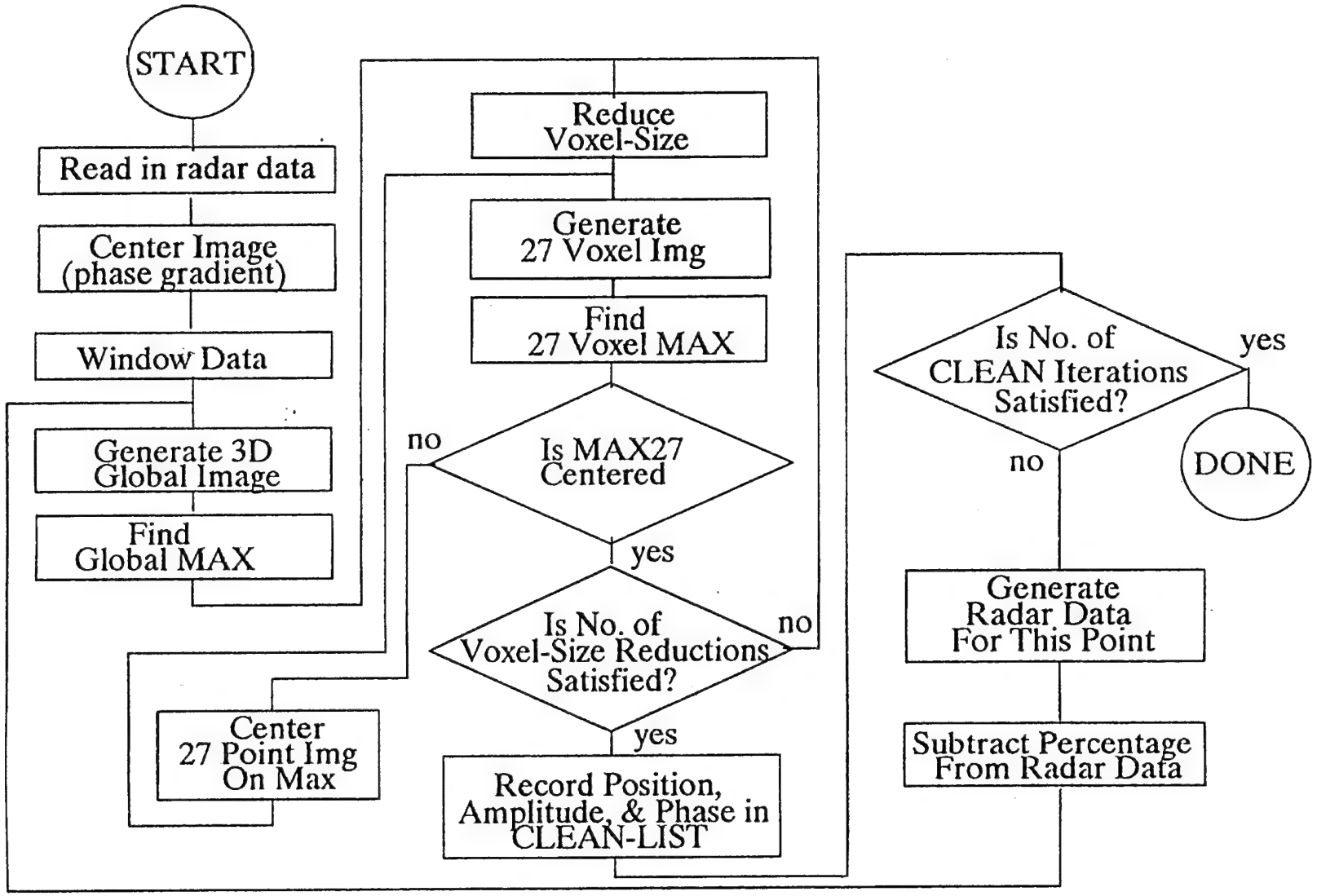

Fig. 2.5 CLEAN Program Flowchart

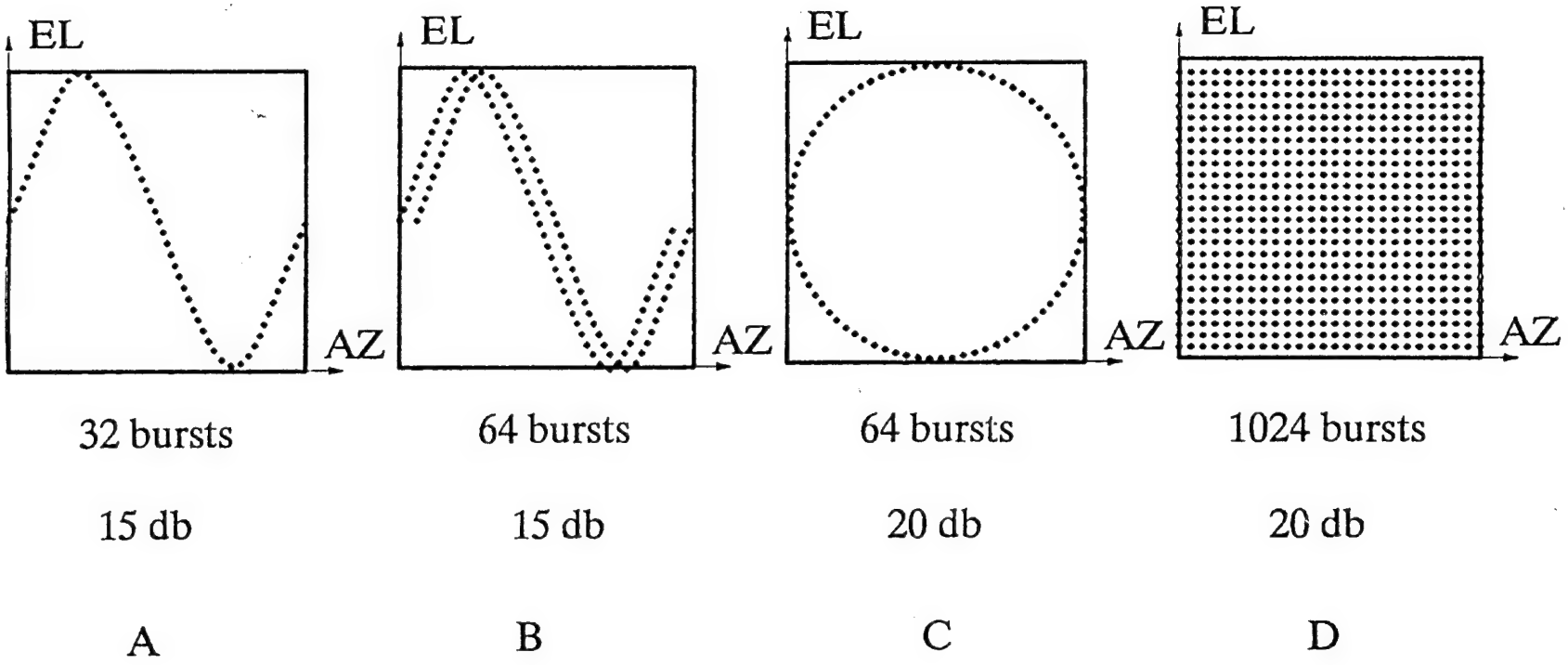

Fig. 3.1 Subapertures and results

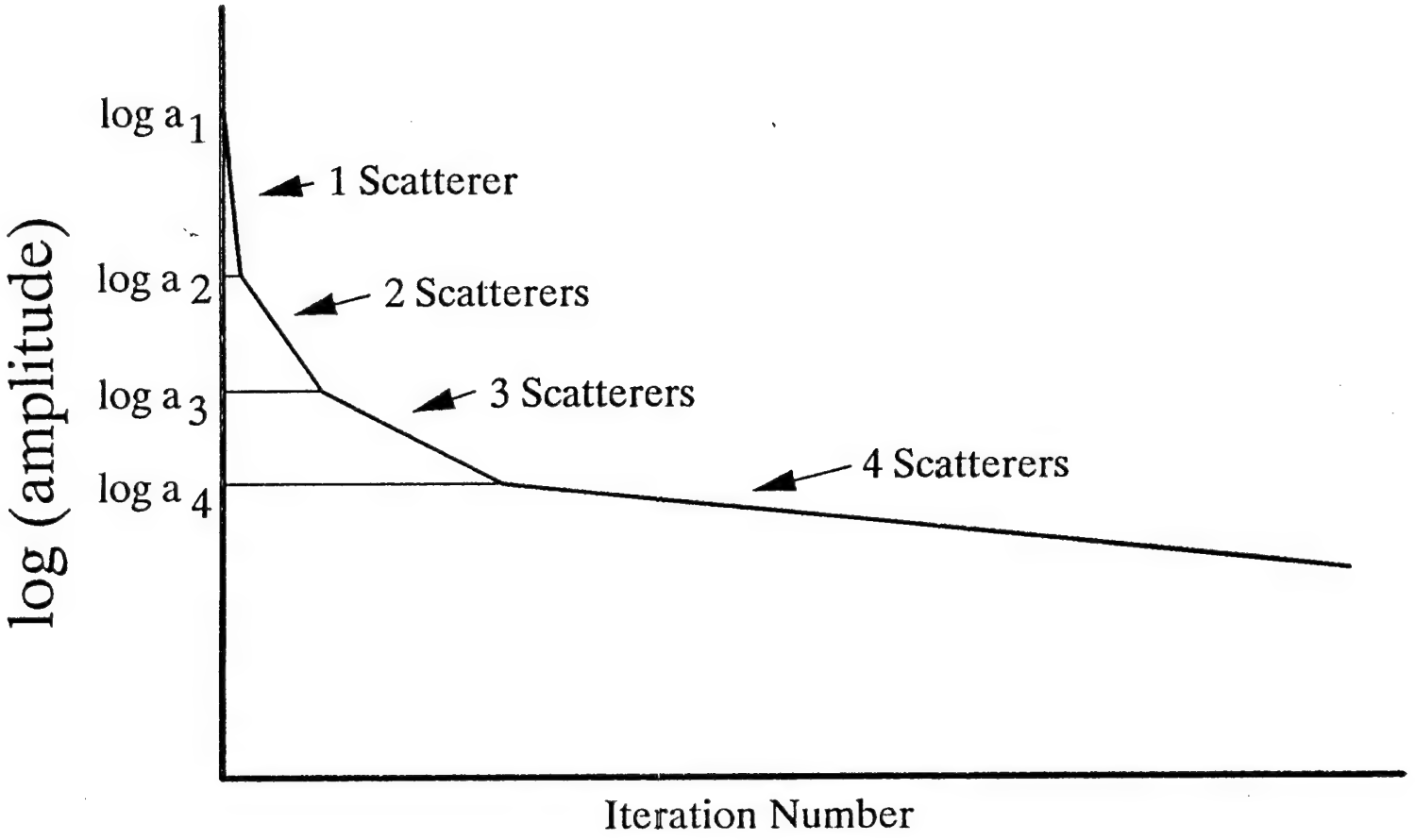

Fig. 3.2 Ideal decrement in image amplitude as a function of iteration number for four scatterer image.

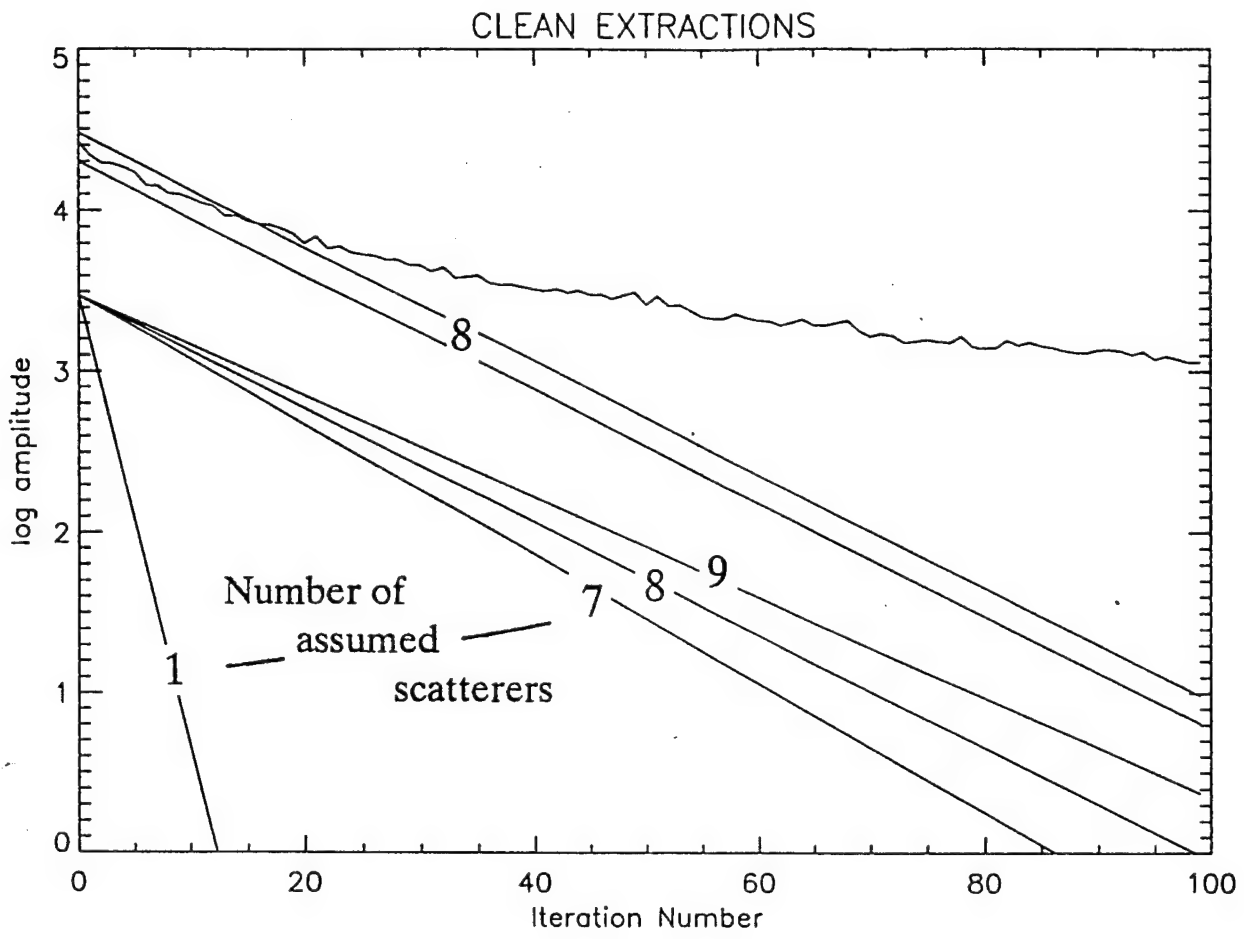

Fig. 3.3 Decrement in image amplitude as a function of iteration number for 8 scatterer data. Straight lines are idealized slopes for numbers of scatterers indicated. Gain = 0.35, number of bursts = 1024.

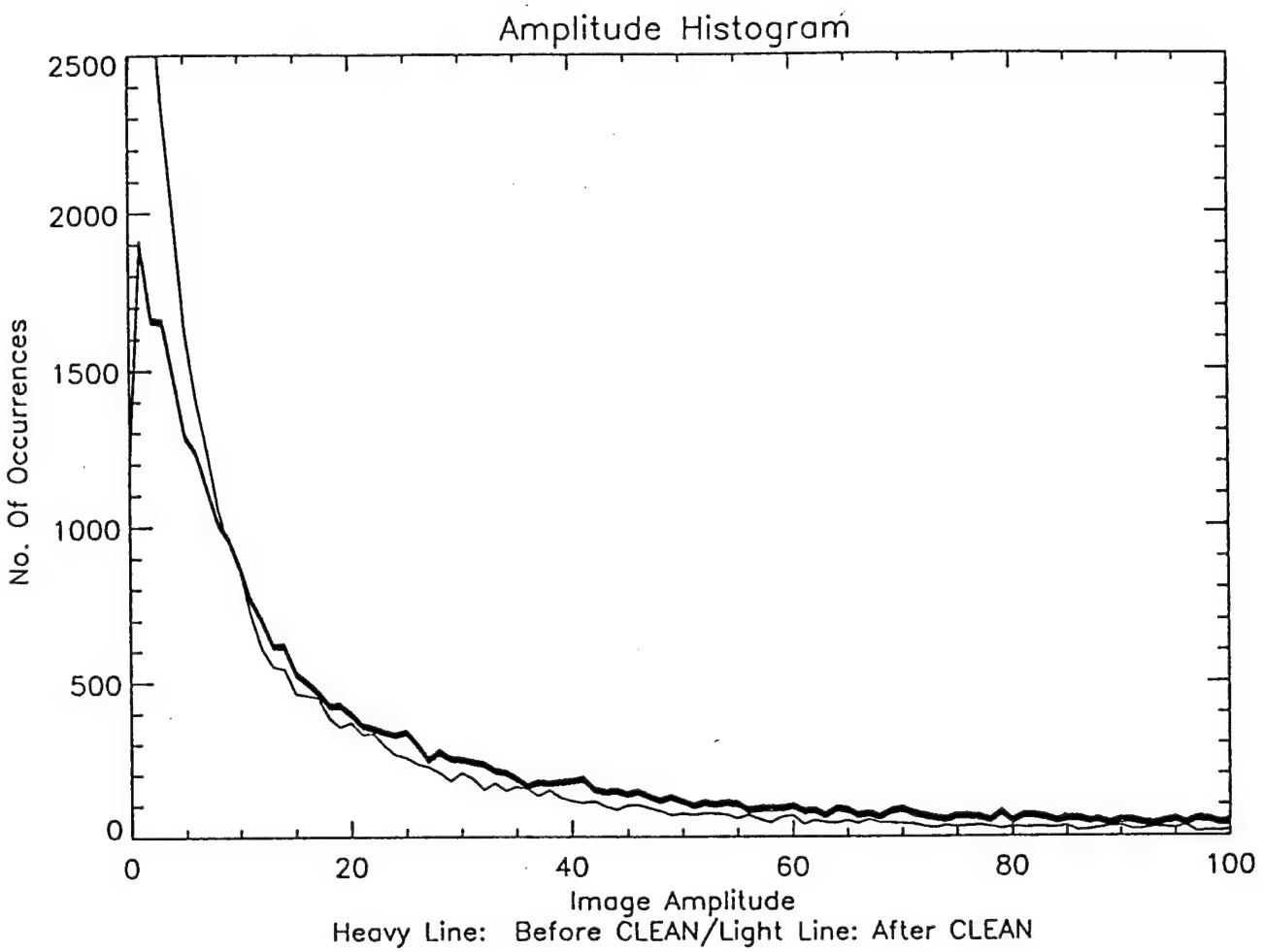

Fig. 3.4 Histogram of amplitudes before and after 25 CLEAN iterations. Data of Fig. 3.3.

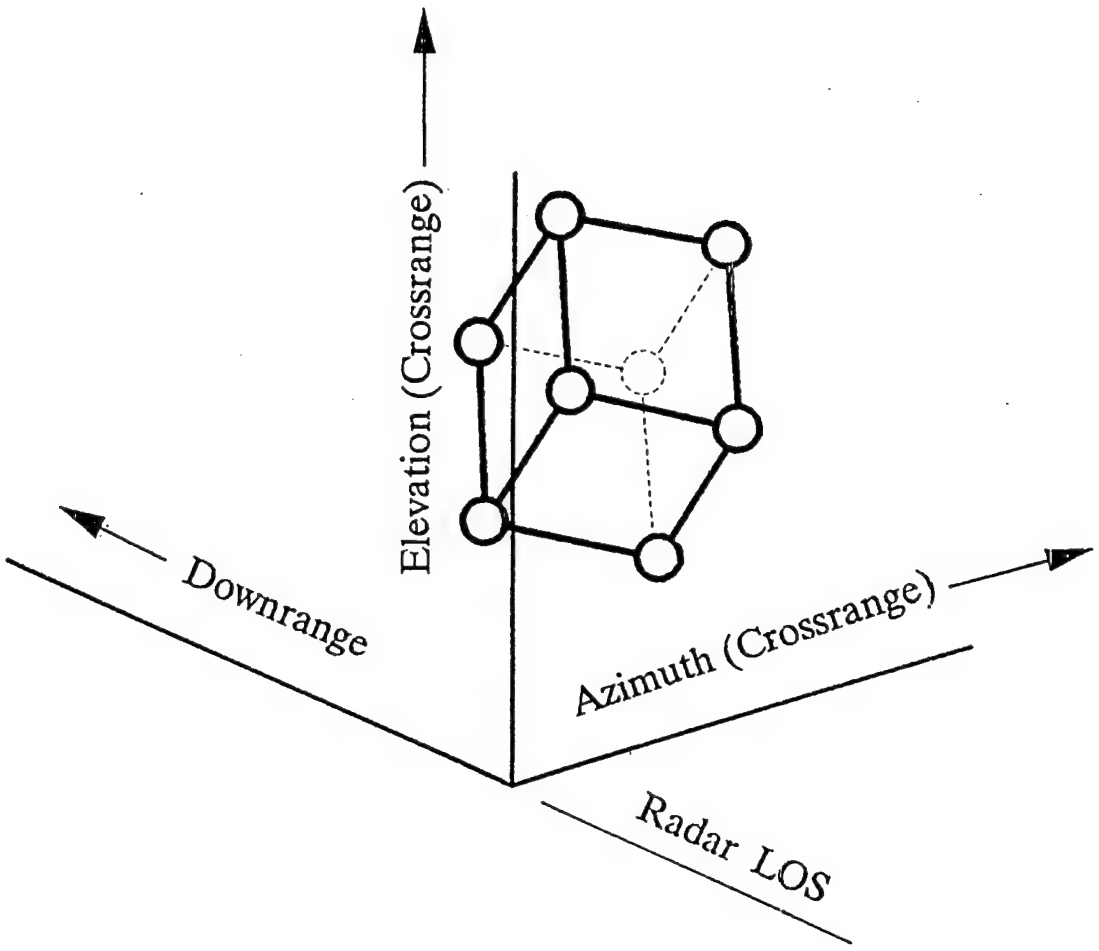

Fig. 4.1 Axis orientation of SLICER (color) images.

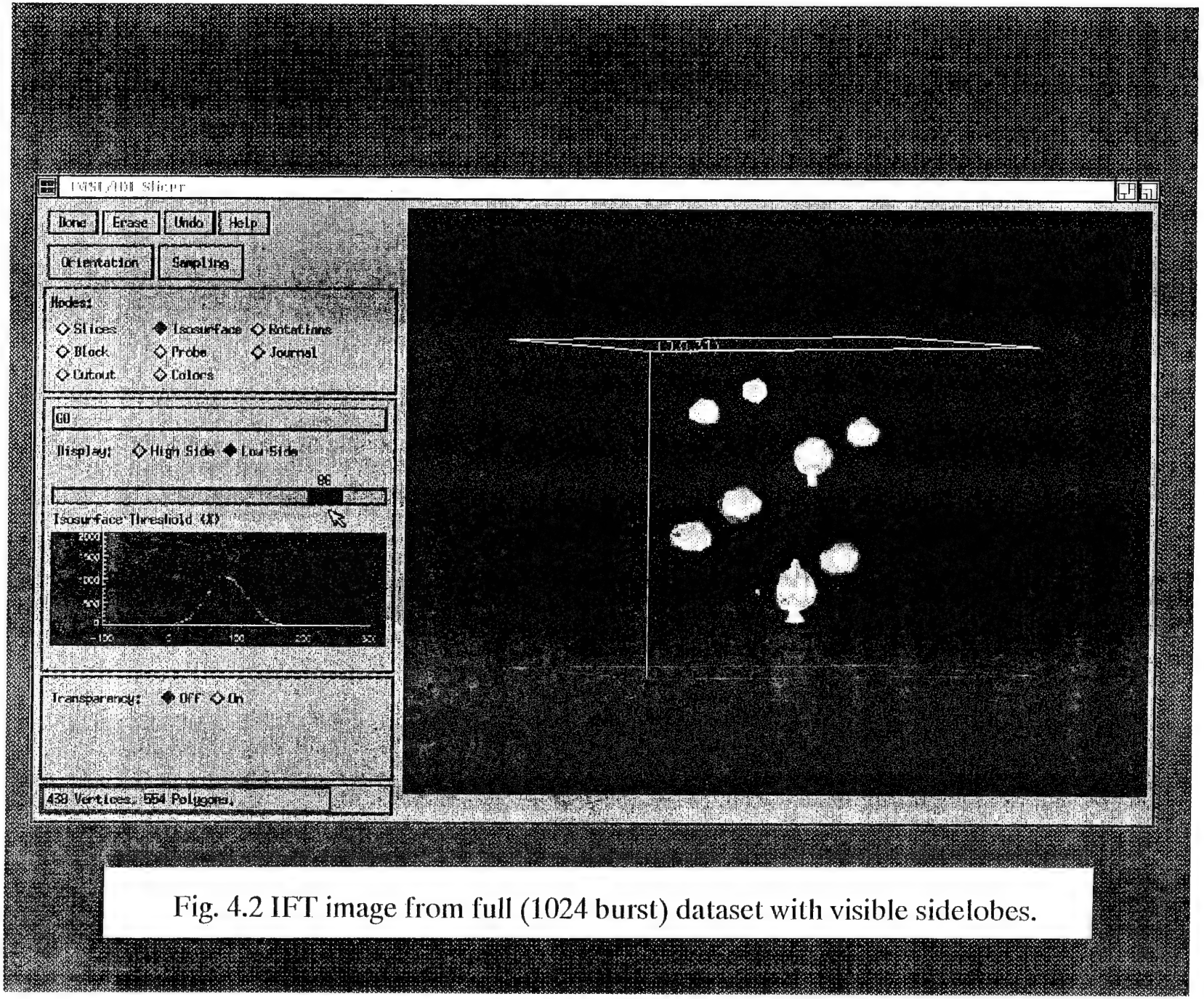

Fig. 4.2 IFT image from full (1024 burst) dataset with visible sidelobes.

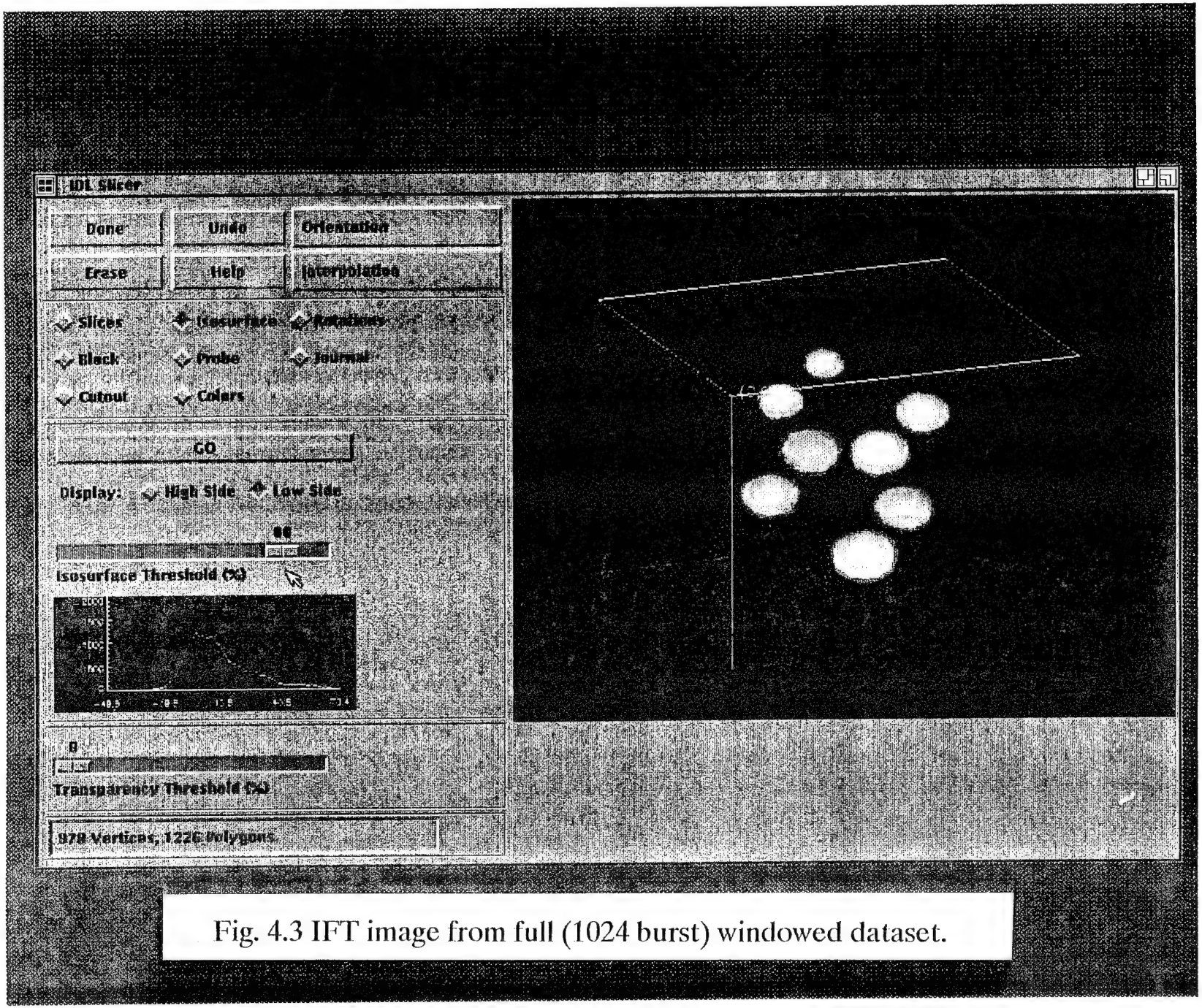

Fig. 4.3 IFT image from full (1024 burst) windowed dataset.

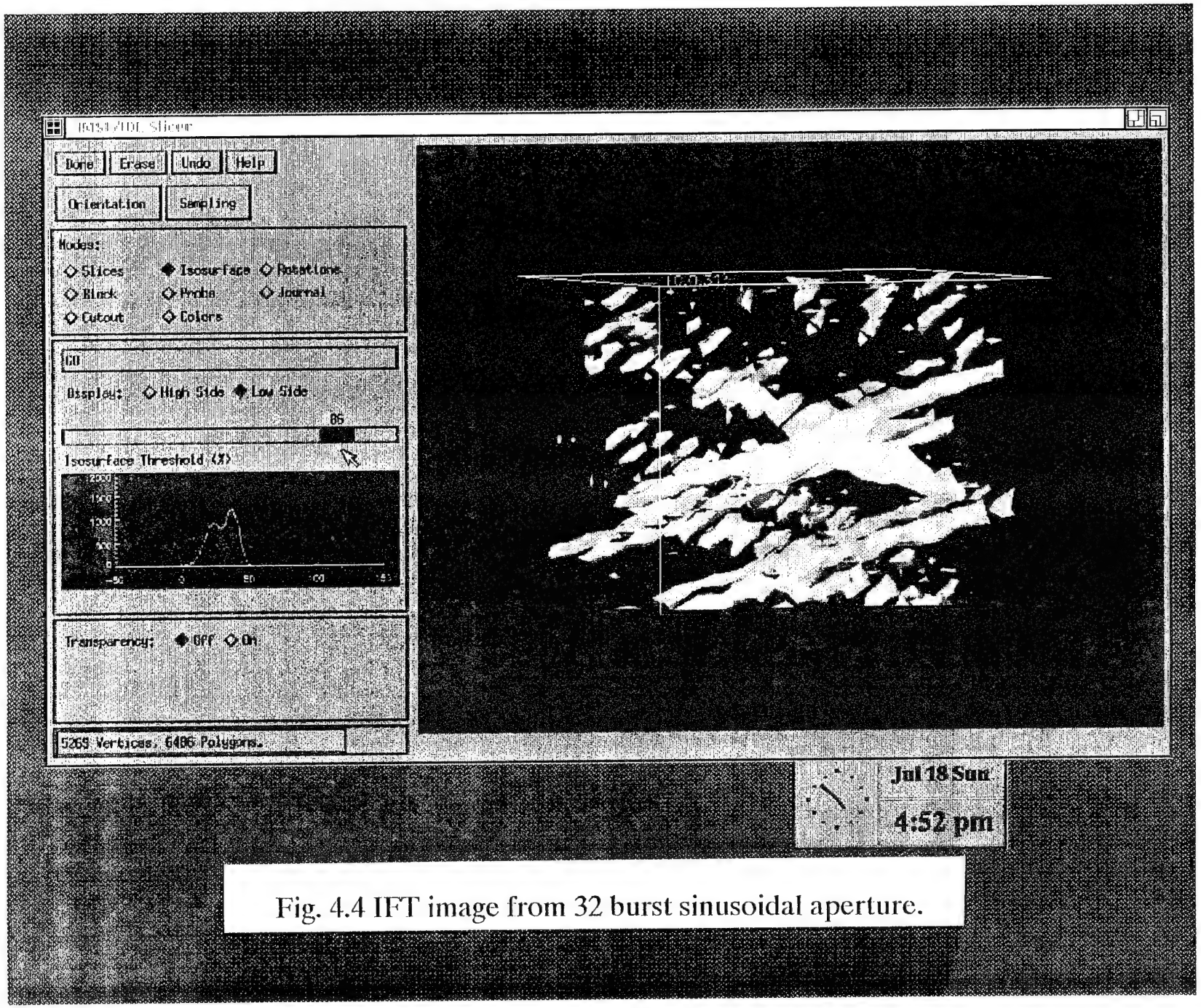

Fig. 4.4 IFT image from 32 burst sinusoidal aperture.

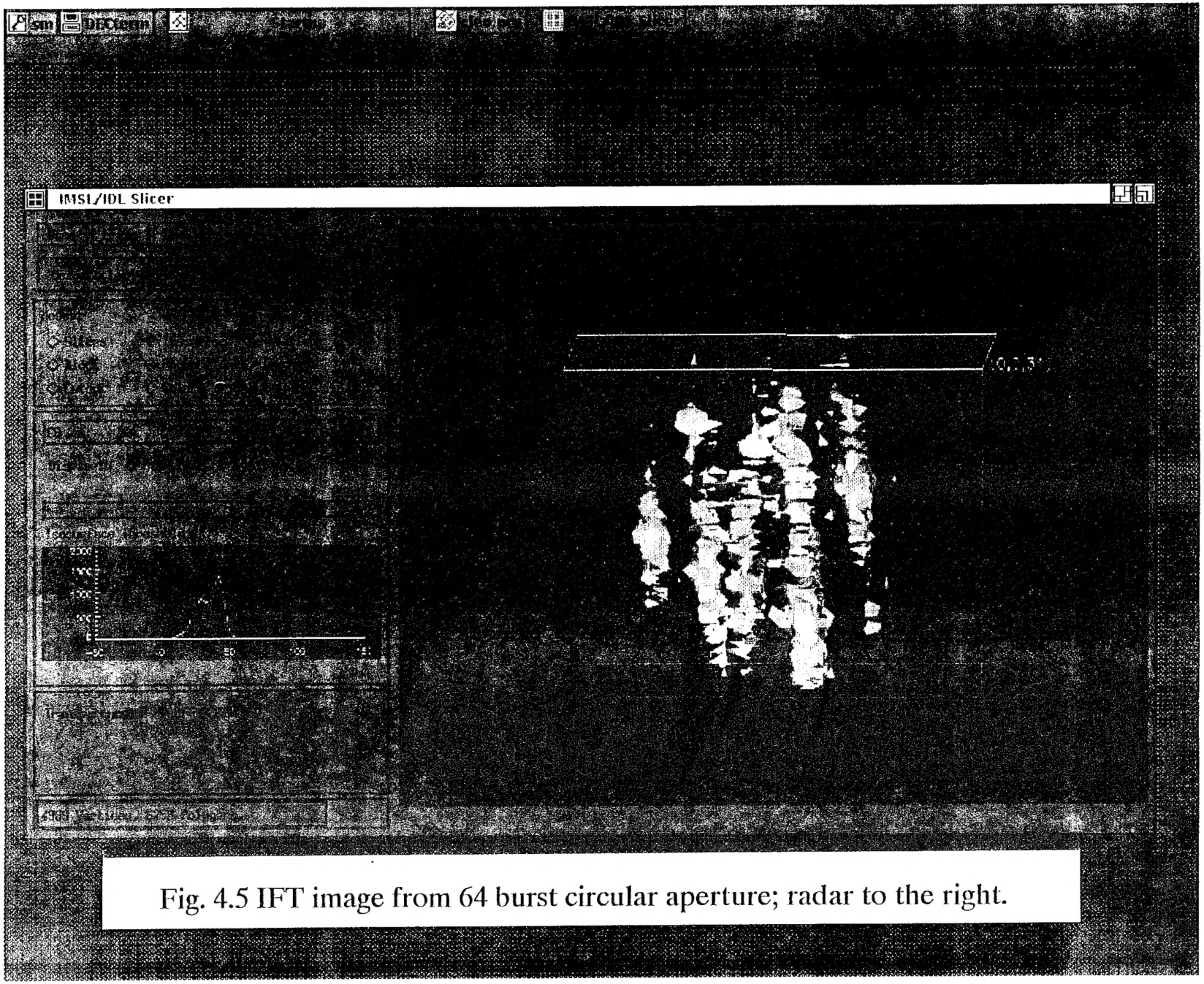

Fig. 4.5 IFT image from 64 burst circular aperture; radar to the right.

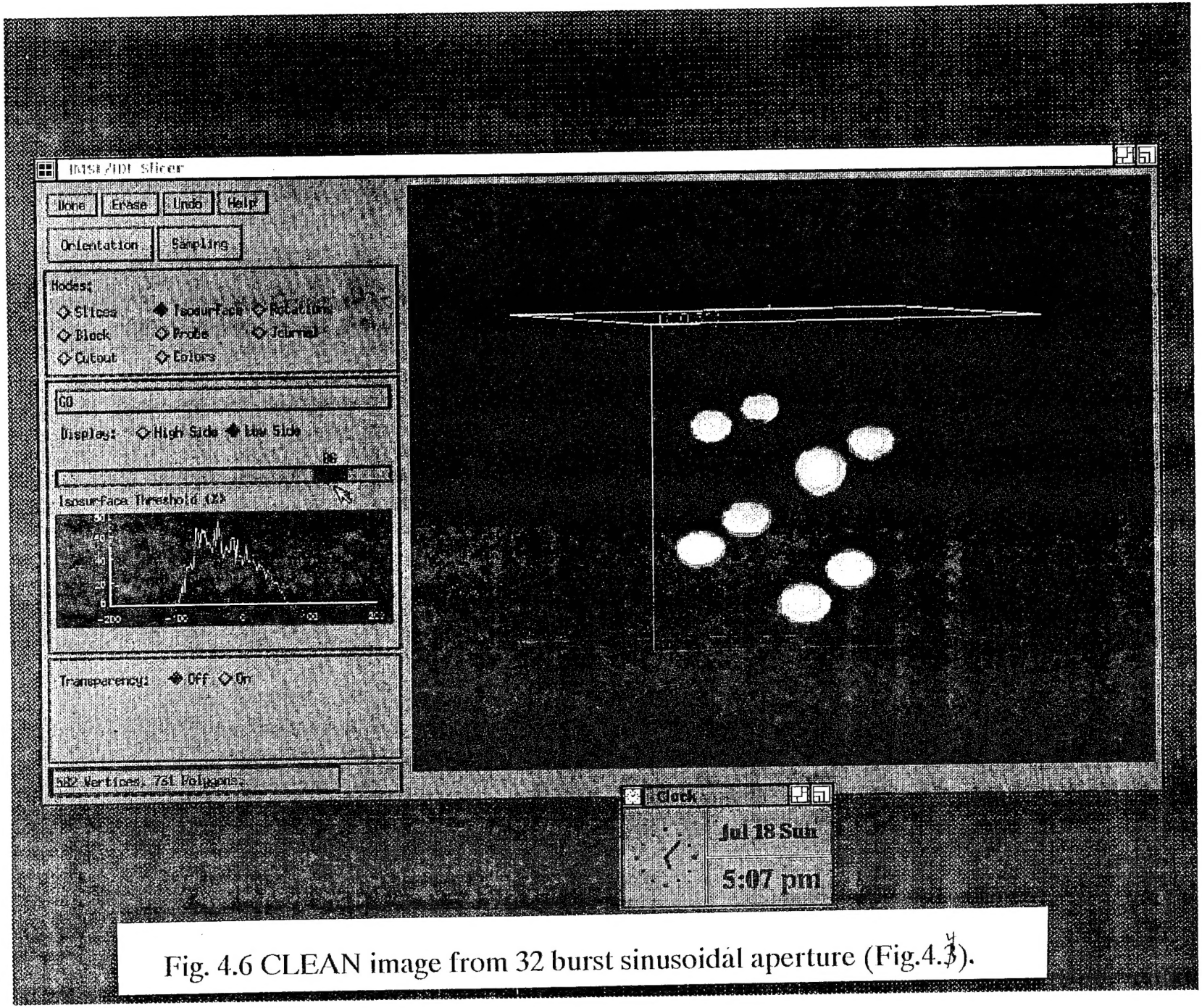

Fig. 4.6 CLEAN image from 32 burst sinusoidal aperture (Fig.4.3).

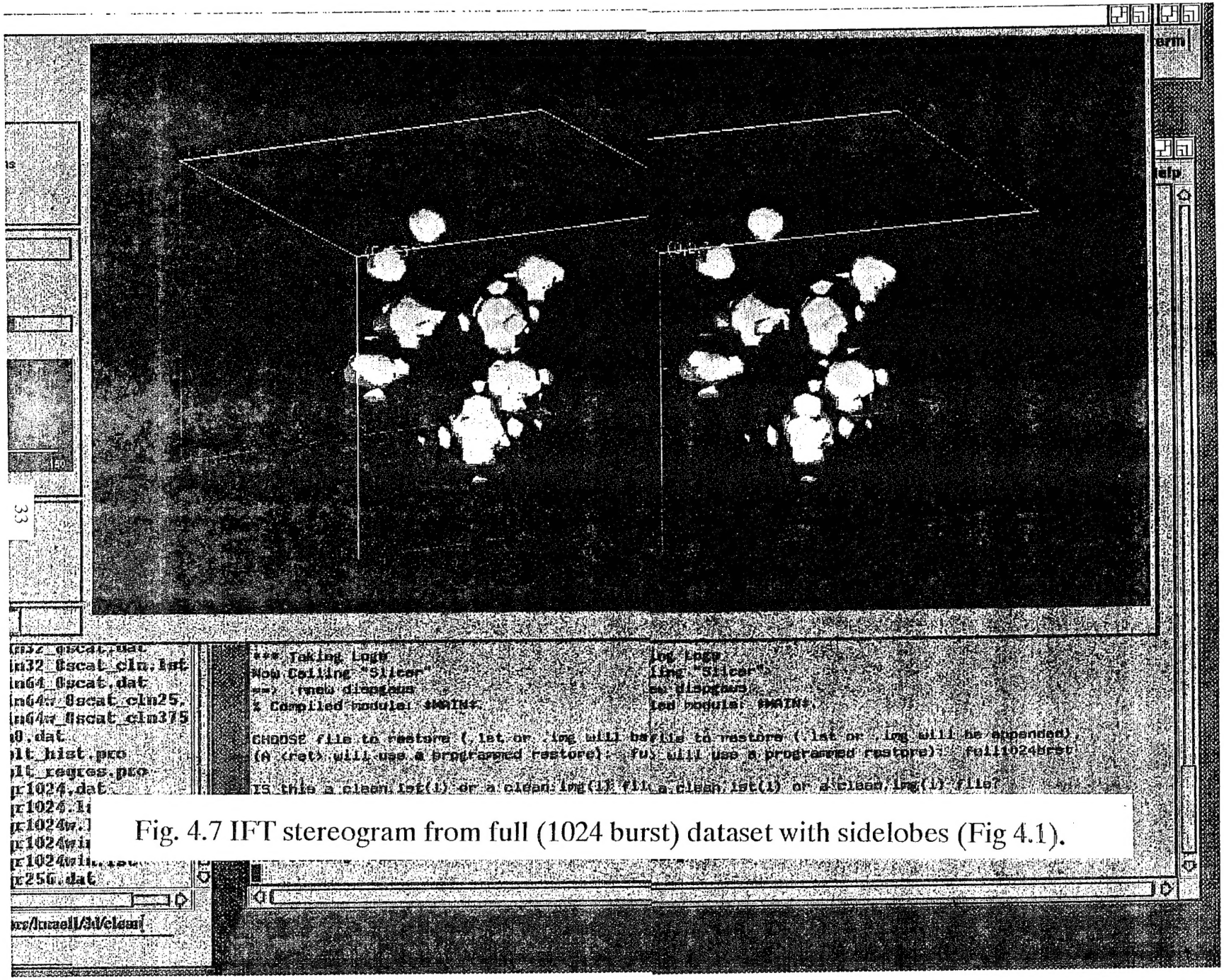

Fig. 4.7 IFT stereogram from full (1024 burst) dataset with sidelobes (Fig 4.1).

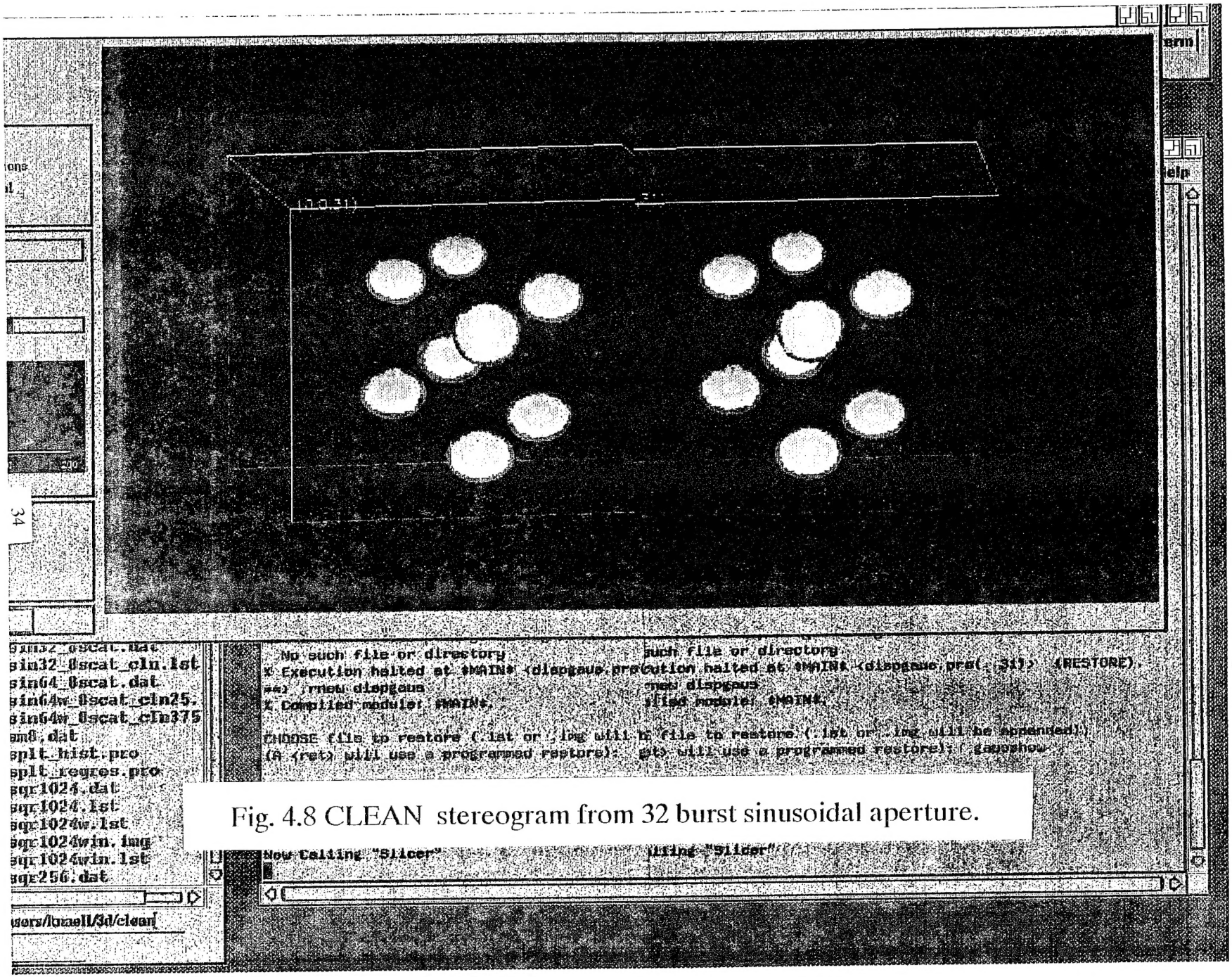

Fig. 4.8 CLEAN stereogram from 32 burst sinusoidal aperture.